CHALMERS
UNIVERSITY OF TECHNOLOGY

CFD simulation of the Wakejet flow

Master's Thesis in Naval Architecture and Ocean Engineering

Hampus Martinsson
Johannes Varosy

Department of Mechanics and Maritime Sciences (M2)
CHALMERS UNIVERSITY OF TECHNOLOGY
Göteborg, Sweden 2017

Report Number X-17/373

CFD simulation of the Wakejet flow

Hampus Martinsson
Johannes Varosy

Department of Mechanics and Maritime Sciences (M2)
Division of Marine Technology
Chalmers University of Technology
Göteborg, Sweden 2017

CFD simulation of the Wakejet flow
HAMPUS MARTINSSON
JOHANNES VAROSY

Supervisor and Examiner :
Arash Eslamdoost, Department of Mechanics and Maritime Sciences (M2)

Report Number X-17/373
Department of Mechanics and Maritime Sciences (M2)
Division of Marine Technology
Chalmers University of Technology
SE-412 96 Göteborg
Telephone +46 31 772 1000

Cover: The Wakejet (Radinn AB, 2016)

Typeset in LaTeX
Printed by Chalmers Reproservice
Göteborg, Sweden 2017

CFD simulation of the Wakejet flow
HAMPUS MARTINSSON
JOHANNES VAROSY
Department of Mechanics and Maritime Sciences (M2)
Chalmers University of Technology

Abstract

The Wakejet is a wakeboard with an electrical powered waterjet unit. It is developed by the Swedish company Radinn AB in Malmö. The company aims to develop an updated series of the Wakejet and would like to analyse the flow both inside the waterjet and around the board, as no previous simulations have been conducted.

The objective for this thesis is to analyse the Wakejet using the commercial CFD-software STAR-CCM+ and try to find areas where improvements can be done. The simulations are performed on the entire Wakejet using free surface simulations as well as on a simplified model of the waterjet unit only. To validate the simplified set-up a validation study is performed on the AxWJ-2 waterjet pump from John Hopkins University where data from physical experiments are available.

Calculations made on the simplified waterjet pump model show that the Wakejet's waterjet pump has a maximum efficiency of 63% at a board speed of 15 knots. On the maximum speed, 25 knots, the efficiency is found to be as low as 25%. The waterjet experiences high amounts of tip leakage blockage at low speeds. Moreover, the design of the stator should be reconsidered since large amounts of separation is found on the pressure side of the blades. Simulation results from the Wakejet model also show that the shape of the intake channel causes a non-uniformity of the inflow to the impeller which should be addressed. On the bright side, the intake grills do not seem to affect the impeller inflow significantly.

Keywords:
Computational Fluid Dynamics, STAR-CCM+, Waterjet, Axial pump, Wakejet, Radinn, AxWJ-2, Cavitation, Tip clearance, Intake grill

Preface

This thesis is a part of the requirements for the master's degree in Naval Architecture and Ocean Engineering at Chalmers University in Göteborg, Sweden. The project has been carried out at the Department of Mechanics and Maritime Sciences (M2) at Chalmers university of Technology together with Radinn AB in Malmö, Sweden, between January and June 2017.

We would like to thank our supervisor and examiner, Ph.D Arash Eslamdoost, from the Department of Mechanics and Maritime Sciences (M2) for his expertise and guidance. We would also like to express our gratitude towards Radinn, especially our main contact Alexander Lind, for giving us the opportunity to work with this project. Thanks also to Joseph Katz and Huang Chen at John Hopkins University for providing us with data and CAD model of their AxWJ-2 axial waterjet pump.

Göteborg, June 2017
Hampus Martinsson and Johannes Varosy

Nomenclature

- Ω - Angular velocity of impeller, [rad/s]
- σ - Cavitation number
- ρ - Density, [kg/m^3]
- ϵ - Dissipation, [m^3/s^2]
- η - Efficiency
- ϕ - Flow rate coefficient
- ψ - Head rise coefficient
- ν - Kinematic viscosity, [m/s^2]
- ω - Specific turbulent dissipation rate, [1/s]
- V_1, V_2 - Inlet velocity, Outlet velocity, [m/s]
- V_s - Ship (Wakejet) speed, [m/s]
- k - Kinematic energy, [m^2/s^2]
- p_1, p_2 - Inlet pressure, Outlet pressure, [Pa]
- p_v - Vapour pressure, [Pa]
- y^+ - Wall distance (non-dimensional)
- H - Head rise, [m]
- Q - Flow rate, [m^3/s]
- T - Torque, [Nm]
- Th - Thrust, [N]
- h - Tip clearance, [m]
- n - Revolutions per second

Abbreviations

- CAD - Computer Aided Design
- CFD - Computational Fluid Dynamics
- CLF - Courant Number
- DOF - Degrees of Freedom
- HRIC - High-Resolution Interface Capturing
- ITTC - The International Towing Tank Conference
- MRF - Moving Reference Frame
- NaI - Sodium Iodide
- RANS - Reynolds-Averaged Navier-Stokes
- RBM - Rigid Body Motion
- RPM - Revolutions Per Minute
- SST - Shear Stress Transport
- TLV - Tip Leakage Vortex
- VOF - Volume of Fluid

Contents

1 Introduction **1**
1.1 The waterjet propulsion system . . . 1
1.2 The Wakejet . . . 3
1.3 Objective . . . 4
1.4 Overview of methodology . . . 4
1.5 Limitations . . . 5

2 Literature Review **7**

3 Theory **9**
3.1 Acting forces and moments . . . 9
3.1.1 Moment of inertia . . . 9
3.2 Waterjet properties . . . 10
3.2.1 Head rise . . . 10
3.2.2 Characteristic velocities . . . 11
3.2.3 Efficiency of a waterjet unit . . . 12
3.2.4 Outlet flow . . . 13
3.2.5 Separation and limiting streamlines . . . 14
3.3 Impeller properties . . . 15
3.3.1 Tip clearance . . . 16
3.3.2 Cavitation . . . 17
3.4 STAR-CCM+ properties . . . 19
3.4.1 Meshing techniques . . . 19
3.4.2 Turbulence model . . . 21
3.4.3 Courant number . . . 22
3.5 Main particulars of the Wakejet . . . 23

4 Methodology **25**
4.1 Preparation of CAD geometry . . . 25
4.1.1 Repairing the pump . . . 26
4.2 Set-up of Wakejet simulation . . . 27
4.2.1 Setting up the domain . . . 27
4.2.2 Splitting the geometry . . . 28
4.2.3 Meshing . . . 29
4.2.4 Computational models . . . 30
4.2.5 Pump modelling . . . 31
4.2.6 Wakejet motions . . . 32
4.2.7 Solvers and convergence criteria . . . 33
4.2.8 Post processing . . . 34
4.3 Set up of AxWJ-2 validation simulation . . . 35
4.3.1 Cavitation study . . . 37
4.4 Set-up of Wakejet pump simulation . . . 38
4.4.1 Inlet velocity to the impeller . . . 39
4.4.2 Impeller tip clearance study . . . 39

4.4.3 Evaluation of simulation technique 39
4.5 Pump studies 40

5 Results 41
5.1 Validation of AxWJ-2 performance 41
5.1.1 Mesh quality 41
5.1.2 Pump performance curves 42
5.1.3 Pump flow 43
5.1.4 Cavitation 47
5.2 Wakejet pump performance 48
5.2.1 Mesh quality 48
5.2.2 Pump performance curves 49
5.2.3 Pump flow 50
5.2.4 Cavitation 54
5.3 Wakejet performance 55
5.3.1 Mesh quality 55
5.3.2 Free surface 56
5.3.3 Intake grill study 58
5.3.4 Cavitation 59

6 Discussion 61
6.1 Validation of AxWJ-2 performance 61
6.2 Wakejet pump study 63
6.3 Wakejet study 65

7 Conclusions 67

8 Future work 69

A Appendix I
A.1 Mesh values I
A.2 Physical conditions II
A.3 Solver properties and stopping criteria III
A.4 Effect of impeller tip clearance IV
A.5 Mesh size and quality IV
A.6 Free surface V

1 Introduction

This section briefly describes the usage of waterjets as a propulsion system and the general principle of today's waterjets. The background and objectives of the project are presented together with a summary of the methodology and limitations.

1.1 The waterjet propulsion system

The waterjet is mostly used on high speed crafts as it is possible to achieve higher propulsive efficiency at high velocities in comparison with vessels equipped with a conventional propeller. Waterjets are typically installed on crew boats, pilot boats and to some extent passenger ferries and pleasure crafts (Borret and Rae, 2008).

The manoeuvrability of a vessel can be improved with waterjets in comparison to the conventional propeller, especially if the vessel is equipped with several steerable waterjets providing a great turning moment. Waterjets can also be equipped with a reversing bucket which redirects the flow and thus enables reversing without reversing the engine.The risk of cavitation is also lower at high velocities for the waterjet system (Faltinsen, 2005). Another benefit is the capability of going in shallow waters.

The drawbacks of the waterjet propulsion system is typically a lower efficiency at lower speeds as well as the risk of injection of objects, such as stones, sea weed or similar, into the intake that could get tangled onto the impeller or in the worst case damage parts of the system. To prevent this many waterjet intakes, including the Wakejet's, are fitted with a form of net or grillage to prevent objects from entering the system. The drawback of this type of protection is that it can disturb the inflow to the impeller (Griffith-Jones, 1994).

Today's waterjets are often divided into four different sections as described in Figure 1.1. The intake, the impeller, the stator and the nozzle.

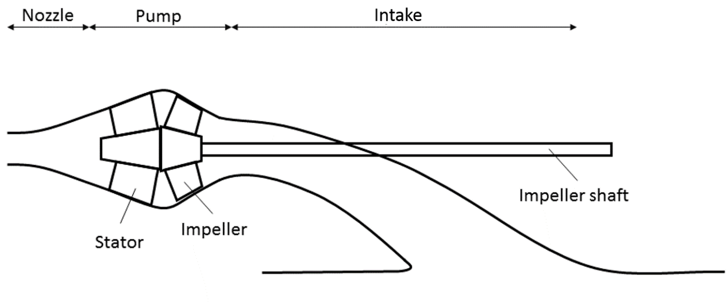

Figure 1.1: Outline of a waterjet system, seen from the side.

The flow enters from the surrounding environment via the intake and continues its path to the impeller where the flow is accelerated by the rotations of impeller via the impeller shaft that is connected to a motor.

The intake should ideally create a uniform flow field to the impeller independent of the running conditions. This could be achieved by controlling the geometry of the intake. This is however a quite complex solution and it is most common for the geometry to have a fixed position (Borret and Rae, 2008). The intake will instead have to be designed to fit the most common running conditions to ensure a higher overall efficiency (Faltinsen, 2005). There are generally three common types of intakes, the flush intake, the ram intake and the scoop intake. The flush intake is by far the most common one, here the intake is more or less parallel to the flow at the intake which means no or very little appendage drag. It could however suffer from air entering the intake and thus a loss of thrust (van Terwisga, 1996). The three intake types can be seen in Figure 1.2 (Eslamdoost, 2014).

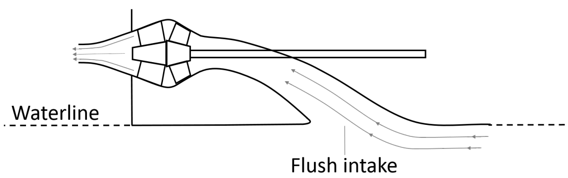

(a) Flush intake.

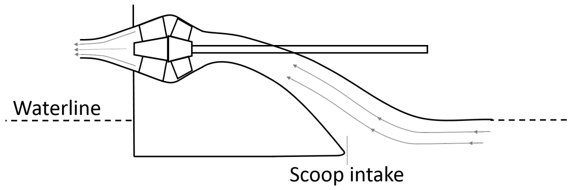

(b) Scoop intake.

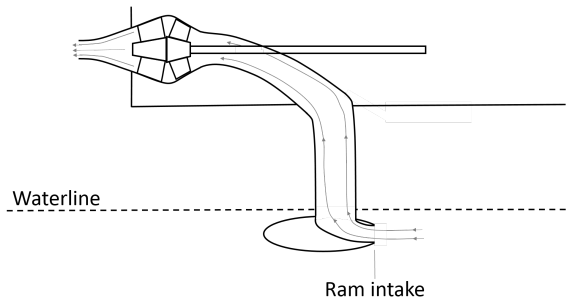

(c) Ram intake.

Figure 1.2: Illustrations of the three common intake types for waterjet systems.

Moreover, waterjets can be divided into axial, centrifugal and mixed flow pumps. They are defined based on the angle between the inflow to the impeller and the outflow from it. For axial flow pumps the inflow to the impeller is parallel to the outflow, i.e. axial. In the centrifugal pump the outflow is orthogonal to the inflow. The mixed flow is a blend between the two previous pump types but are more often compared to the axial flow pumps. The impeller is thus designed in different ways depending on the type of pump used (Carlton, 2012). The impeller can just like an conventional propeller be optimised to increase the efficiency as well as to avoid cavitation. This can be done by changing the number of blades and altering the blade pitch. Axial impeller are usually have four to eight blades (Carlton, 2012).

The aim of the stator is to minimise the swirl of the flow downstream of the impeller. Since the aim is to have all outflow going purely in the axial direction in order to gain maximum thrust. The nozzle is adding further momentum to the jet flow and is often designed so that outlet flow is as uniform as possible. The stator cone further helps to avoid separation downstream of the stator and should help the flow to be uniform in the outlet (Carlton, 2012).

1.2 The Wakejet

The Wakejet is a wakeboard equipped with an electrically powered waterjet unit. It is designed by Radinn AB, a Swedish company located in Malmö. Radinn's vision is to revolutionise action sports through radical innovation. The Wakejet Cruise, which can be seen in Figure 1.3, is designed to be fun for all but is not intended to operate in extreme water conditions. The Wakejet has a maximum speed of 25 knots and a impeller rotating at a design speed of 6500 RPM. The typical usage of the Wakejet is to go as fast as possible during the 20 minutes of run time before the battery pack is drained and needs to be charged. Unfortunately, no data on driving pattern is available but it it fair to say that the operational hours that a Wakejet is used during its lifetime are low. The next version will be called the Wakejet Freestyle and is designed to be used in rapids, waves and even on wakeboard kickers and sliders. The Wakejet Cruise, has been hand shaped and developed through trial and error but in order to create a new model that is faster, lighter, has longer battery life and is more agile, Radinn needs to analyse and evaluate the design in more detail (Radinn AB, 2017).

Figure 1.3: The Wakejet (Radinn AB, 2016).

The waterjet system fitted on the Wakejet has a flush intake, an axial pump with four blades and a stator with six blades. Moreover, the intake is fitted with two intake grills in order to keep the pump system free of disturbing objects. The Wakejet is 1.9m long, has a maximum breadth of 0.8m and a height of 0.18m. The waterjet impeller diameter is 90mm.

1.3 Objective

The main purpose of this project is to analyse the flow around the Wakejet and inside its waterjet unit to find areas where the overall efficiency could be improved. The focus should primarily be on the waterjet unit and the geometry surrounding it.

To analyse the Wakejet performance a number of different studies need to be conducted (presented in no particular order):

- Pump performance curves at different flow rates
- The risk of cavitation on the impeller
- Evaluation of tip clearance losses for different tip clearances as well as risk of flow blockage
- Estimation of effect on inflow to the impeller due to the intake grills
- Self-propulsion simulations
- Analysis of limiting streamlines on the impeller and stator

1.4 Overview of methodology

In the beginning of the project, a thorough literature study is conducted to get an overview of how waterjets are modelled in Computational Fluid Dynamics (CFD) today as well as on needed theory to calculate parameters such as efficiency. If possible, articles regarding fluid dynamics of similar projects such as surfboards, wakeboards or personal water crafts are analysed.

Before setting up the CFD simulations the geometry must be simplified so that it is water tight and cleaned of parts that doesn't effect the flow around the hull (eg. parts inside the board such as the battery). These alterations are performed using the Computer Aided Design (CAD) softwares Rhino 5 and Catia V5.

When the geometry is prepared the simulations can be set up in the CFD code STAR-CCM+. Two different models are created for the Wakejet: One consisting of the entire Wakejet in a Volume of Fluid (VOF) domain simulating a free surface. The second model consists only of the impeller, impeller shaft, stator and nozzle using a single fluid model to evaluate the pump performance. Validations of the simplified simulations are conducted using the same set-up for an axial waterjet pump from John Hopkins University called "AxWJ-2" where performance curves are available. All simulations are conducted using the two equation turbulence model $k-\omega$ SST.

1.5 Limitations

The limitations of the project is first of all the time frame, the project will run from January 2017 until June 2017 and corresponds to 30 credits per person at Chalmers University of Technology. STAR-CCM+ will be the only CFD-code that will be used to perform simulations. In STAR-CCM+ the only turbulence model that is used is the $k - \omega$ SST two equation turbulence model.

Simulations on the Wakejet will only be performed in calm water conditions for speeds between 5 to 25 knots. No other degree of freedom will be allowed other than translation in the vertical direction. Moreover, only one weight (75kg) of the person riding the Wakejet will be evaluated. The Wakejet-board will not be redesigned other than small alterations to make the geometry water tight and compatible with STAR-CCM+.

The waterjet system will be simulated separately and some alterations to the geometry will be done to reduce the number of cells. The tip clearance of the impeller will be changed to investigate the effects on the waterjet performance, otherwise no redesign will be done.

The Wakejet will not be tested physically in any other way than through a test ride due to lack of testing facilities and measuring equipment.

2 Literature Review

In the beginning of the project a thorough literature study is conducted. In this section the most interesting sources are summarised in chronological order.

Griffith-Jones (1994) discusses the use and effect of intake grills at the intake to a waterjet pump. The thesis shows that, for the given pump, intake grills reduces the separation region in the channel considerably and thus increases the efficiency. On the other hand, the pressure at the impeller plane is considerably lower for the case with intake grills, making the pump work harder to keep up with the volume flux. The two effects counteract each other and the exact effect of the intake grills was hard to quantify.

Moon-Chan and Ho-Hwan (2005) investigates how changing the duct diameter and thus changing the tip clearance (h) affects the efficiency of an axial-flow type waterjet. Two different gap ratios were tested 1.5% and 0.7% (made dimensionless by the impeller diameter). The results from this study concludes that the performance of the waterjet is highly dependent on the tip clearance and that the case with h=1.5% showed an overall efficiency around 25% higher than the h=0.7% case.

Bulten and Esch (2007) presents CFD results from calculations on different pump configurations using both Moving Reference Frame (MRF) and the Rigid Body Motion (RBM) simulations and compare them to measurements. They conclude that results from the simulations are close to measured values for both the MRF and RBM rotation techniques.

Michael et al. (2008) covers the design process of the AxWJ-2 axial flow pump. The pump is designed for model testing and its design is based on requirements for high speed vessels. The report also provides efficiency predictions of the pump using CFD software codes CFX and Fluent.

Brizzolara and Villa (2010) shows how a semi-empirical method to evaluate planing hull's performance can be constructed using Savitsky method together with a Reynolds-averaged Navier-Stokes (RANS) solver. CFD simulations are carried out in STAR-CCM+ using a $k - \epsilon$ turbulence model with a double later law of the wall. The paper concludes that RANS solvers are capable to predict the resistance, pressure distribution and flow field of a planing hull in calm waters, even when some small appendages are included. The Savitsky method then takes care of the running behaviour of the hull.

Peri et al. (2012) describes the process of optimising a waterjet driven catamaran using both a high fidelity, unsteady, RANS solver and a Variable Fidelity/Variable Physics approach. ITTC recommendations are used to compare the results. The unsteady RANS solver uses a blended $k-\epsilon$ / $k-\omega$ turbulence model together with a higher order upwind differencing scheme. The article shows that roughly half the computational time can be saved by using the variable physics approach rather than unsteady RANS while getting similar results.

Andersen and Moe (2014) uses a two degrees-of-freedom (DOF) finite element method to investigate the hull-waterjet interaction. A $k-\epsilon$ turbulence model with wall functions is used to simulate the flow. The study includes variations of Froude number (Fn), initial trim and waterjet intake as well as a grid dependence study. The thesis shows that bare hull simulations are valid for high Fn whereas self propulsion simulations are reliable for low Fn. It also shows that the resistance peaks for self propulsion appears at lower Fn than that of bare hull tests. Regarding initial trim, the report shows that it should be zero degrees for design Fn.

Kang et al. (2014) analyses how different number of stator blades matches a certain impeller for an axial-flow pump. This was done using a $k-\epsilon$ turbulence model in the CFD code ANSYS-CFX. The report tested three different number of stator blades: 5,7 and 9. The operational performance of the different cases were evaluated and it was found that the case with 7 blades yielded the highest pump efficiency.

Feldbrugge (2015) shows how two different methods can be applied to STAR-CCM+, the Volume of Fluid (VOF) method and the Single Fluid method, to simulate outlet flow from a waterjet using different impeller blade angles and a steady $k-\omega$ SST turbulence model. It is shown that both methods differ from Direct Numerical Simulation data and that further work in STAR-CCM+ thus needs to be done. The report is ended with a list of recommendations that can be used for further investigations.

Tan et al. (2015) thoroughly explains experimental procedures to determine the performance of the axial waterjet pump AxWJ-2 by using test facilities available at John Hopkins University. The paper also discusses the tip leakage vortices effect on cavitation and overall performance of the pump. It is shown that the interaction between tip leakage and cloud cavitation may cause "cavitation breakdown", i.e. a large decrease in efficiency due to cavitation, at certain inlet pressures.

3 Theory

This chapter presents the theory used to evaluate the performance of the Wakejet and its waterjet unit.

3.1 Acting forces and moments

There are mainly three forces and one moment that are important for analysis of results in this project: Lift, Drag, Torque and Thrust. Torque and Thrust are two forces acting on the impeller whereas lift and drag are calculated over the whole Wakejet body. The drag in this case includes all resistance components acting on the hull as well as the thrust generated by the waterjet. As the Wakejet is mainly operating in the planing region the lift force will consist mainly of the hydrodynamic lift force.

The importance of lift and drag comes in to play for self-propulsion simulations with the whole Wakejet, where the lift force acting on the body should match the weight of board and rider in order to have the Wakejet at the correct waterline. The drag on the other hand is related to the thrust and thus the rotational speed of the impeller. Following Newtons second law, all forces should be equal to zero if the board isn't accelerating. The impeller should thus rotate at such a speed that it generates enough thrust to make up for the resistance forces acting on the Wakejet. In other words, the drag force (total force in the direction that the board is heading) should be exactly zero.

The impeller thrust and torque is important when analysing simulations on only the waterjet unit. Thrust, Th, is the output of the impeller and as much thrust as possible in the forward direction is desirable. Moreover, the torque, T, is the moment around the impeller axis due to the interaction between the flow itself and the impeller. It is thus a loss of energy in the system, as can be seen in Equation 3.4 a high torque will give a low waterjet efficiency.

3.1.1 Moment of inertia

In order to simulate rotation of a body,the moment of inertia of the object needs to be known. However, it is not possible to get the exact value from STAR-CCM+ or any other software available in the project. The moment of inertia is then approximated by calculating the moment of inertia of a solid box with constant density and the same length, breadth and height as the Wakejet. The formulae used are seen in equation 3.1 (Engineers Edge, LLC, 2017).

$$I_x = \frac{m_{tot}}{12}\left(H^2 + B^2\right), \quad I_y = \frac{m_{tot}}{12}\left(H^2 + L^2\right), \quad I_z = \frac{m_{tot}}{12}\left(B^2 + L^2\right) \tag{3.1}$$

Where I_x is moment of inertia around the x-axis of a body centred coordinate system. I_y and I_z are corresponding moment of inertia around the y- and z-axes. L, B and H are the length, breadth and height of the Wakejet. m_{tot} is the total weight of the Wakejet and person riding it.

3.2 Waterjet properties

The output thrust of a waterjet unit is directly coupled to the Momentum Flux throughout the system. One of the uncertainties regarding waterjet calculations is the difficulty to measure the net thrust generated by the impeller in physical tests. Instead, the thrust is calculated indirectly by measuring the flow through a number of different cross section areas defined by the International Towing Tank Conference (ITTC) (Eslamdoost, 2014). However, since this project is entirely conducted through CFD it is possible to get the net thrust directly from STAR-CCM+.

3.2.1 Head rise

A way of measuring the energy that is added to the system by the pump is called Head Rise, H. The head rise is measured in meters and is derived directly from Bernoulli's equation (Equation 3.2).

Figure 3.1 shows a principal waterjet system with an inlet (1) and outlet (2) where velocity, v_i, and pressure, p_i, are measured. Moreover, the outlet is placed a distance, Δ h, above the inlet. By applying Bernoulli's equation the head rise can now be calculated as in Equation 3.3 (Carlton, 2012).

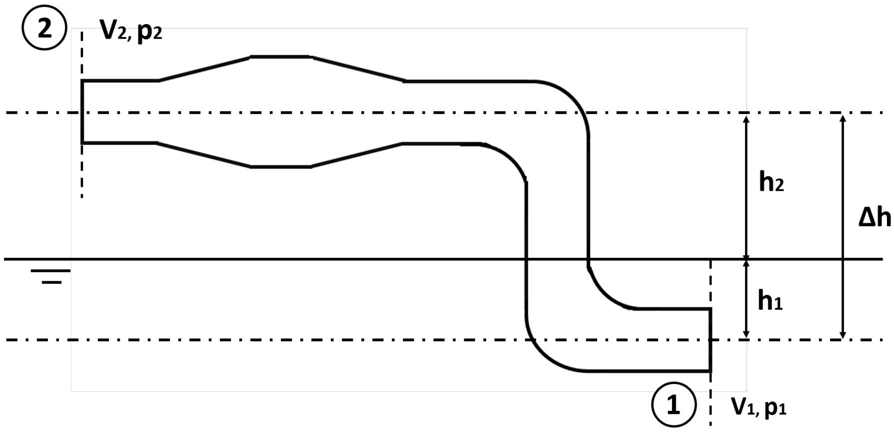

Figure 3.1: Sketch of principal waterjet.

$$\frac{p_1}{\rho g} + \frac{{V_1}^2}{2g} + H = \frac{p_2}{\rho g} + \frac{{V_2}^2}{2g} + \Delta h + h_{loss} \tag{3.2}$$

$$H = \frac{{V_2}^2 - {V_1}^2}{2g} + \frac{p_2 - p_1}{\rho g} + \Delta h + h_{loss} \tag{3.3}$$

The first term at the right hand side of Equation 3.3 represents the dynamic pressure difference and the second term the static pressure difference between the two positions. h_{loss} represents losses inside the system such as friction and can often be neglected (Carlton, 2012).

3.2.2 Characteristic velocities

When looking at a waterjet system it is important to remember that the inlet velocity to the impeller will differ from the ship (or board) velocity, V_s. This is due to the fact that the waterjet system takes water from the boundary layer that is formed around the ship. Figure 3.2 shows how the velocity at the intake, V_{in}, depends on the velocity profile just before the intake. The inlet velocity to the impeller, V_1, is then taken as a surface average just before the impeller whereas the outlet velocity is defined as the average at the outlet plane (Bulten, 2006).

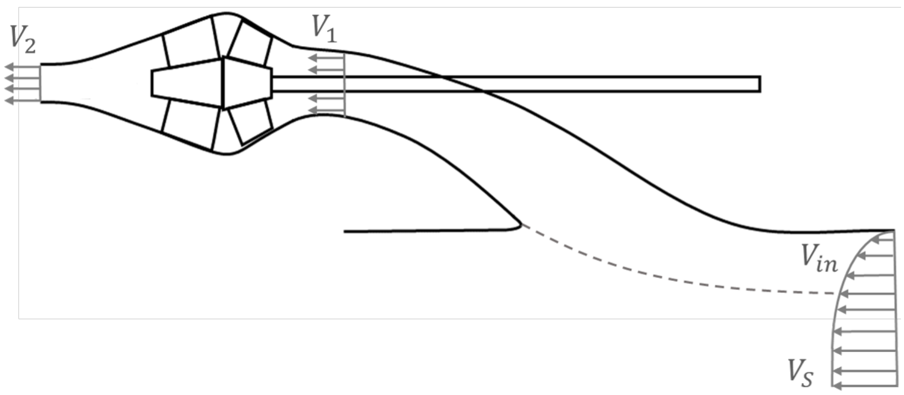

Figure 3.2: Sketch of waterjet system showing difference between V_s, V_{in}, V_1 and V_2.

For fast going ships, typically >60 knots, the ship speed can be over two times faster than V_1. A risk with having a high ratio between V_s and V_1 is that the pressure gradient causing the deceleration of the flow being too high. A high pressure gradient could for a poorly designed intake lead to separation at the top side of the intake channel, affecting the inlet flow to the impeller, as can be seen in Figure 3.3 (Bulten, 2006).

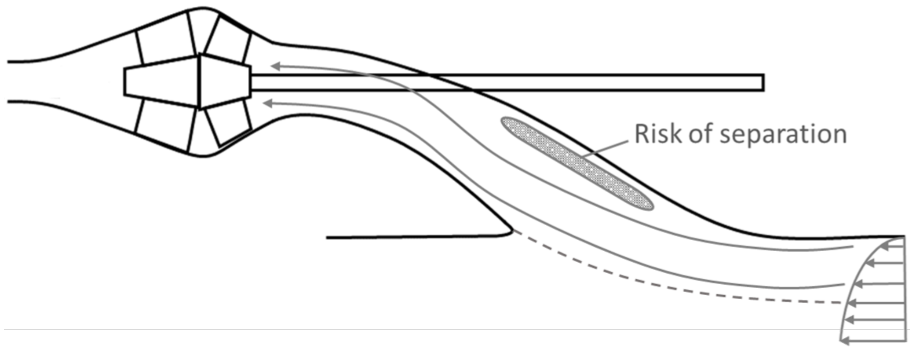

Figure 3.3: Illustration of risk of separation at top side of channel for high ratio between V_s and V_1.

3.2.3 Efficiency of a waterjet unit

According to Miorini et al. (2012), the efficiency of a waterjet unit can be calculated as a relationship between flow rate, head rise, torque and impeller rotational speed as follows:

$$\eta = \frac{\rho g H Q}{T\Omega} \tag{3.4}$$

Where Q is the flow rate through the impeller in m^3/s, H is the head rise as described in equation 3.3, T is the impeller torque and Ω is the angular velocity of the impeller.

To be able to compare different waterjet units, the performance can also be described in terms of non-dimensional flow and head rise coefficients, ϕ and ψ. The two parameters are defined in Equations 3.5 and 3.6. For ϕ, n is the rotational speed of the impeller in rotations per second and D is the inner diameter of the outlet pipe.

$$\phi = \frac{Q}{nD^3} \tag{3.5}$$

For the head rise coefficient ψ, p is the measured pressure and V_i is the measured velocity at the different positions.

$$\psi = \frac{p_2 - p_1 + \frac{\rho}{2}({V_2}^2 - {V_1}^2)}{\rho n^2 D^2} \tag{3.6}$$

3.2.4 Outlet flow

When analysing the outlet flow from any kind of jet system it is desirable to have the entire flow going in the axial direction at the outlet to gain maximum forward thrust. All tangential flow can thus be considered as a loss of kinetic energy. When it comes to a waterjet system, a stator is positioned between the impeller and the outlet which should reduce the tangential velocities, also called swirl, as much as possible. Outlet swirl leads to a pressure drop at the outlet, as defined in Equation 3.7 (Eslamdoost, 2014).

$$\Delta p_{swirl} = -\rho \int_0^R \frac{V_{2\phi}^2}{r} dr \tag{3.7}$$

Where ρ is the fluid density, R is the outlet radius, $V_{2\phi}$ the tangential velocity at the outlet, r the radial distance from the centre of the outlet.

Another important term when regarding jet flows is the vena-contracta. Vena-contracta occurs when the static pressure in the fluid is equal to the ambient pressure. For waterjets this usually means that vena-contracta occurs when the pressure in the water is equal to atmospheric pressure. For a perfectly designed outlet, this will occur exactly at the nozzle, giving a uniform outflow of water. Having a vena-contracta aft of the nozzle also implies that the outflow from the nozzle is not uniform, which is not optimal in order to gain maximum thrust (Eslamdoost, 2014). Figure 3.4 show the case where vena-contracta occurs outside the waterjet boundaries (van Terwisga, 1996).

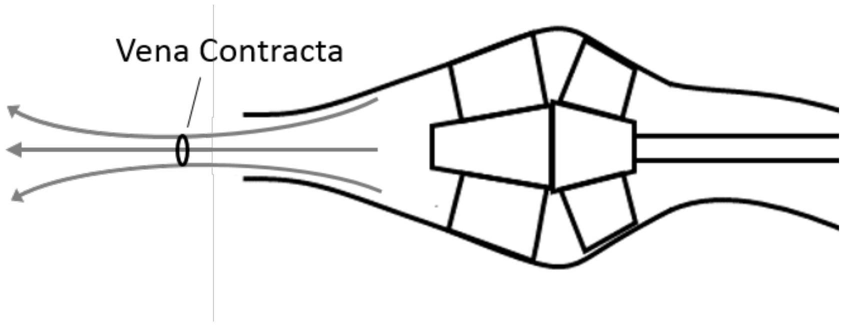

Figure 3.4: Vena-contracta occurring aft of the nozzle.

3.2.5 Separation and limiting streamlines

In a boundary layer flow there are mainly three different forces acting on a fluid element: pressure, inertia and frictional forces. To explain the driving mechanisms of separation an example of a flat plate boundary layer is used.

At the outer edge of the boundary layer the pressure and inertia forces are dominating. At the wall the pressure and frictional forces are dominating. If the static pressure increases and its gradient becomes positive ($\frac{\partial p}{\partial x} > 0$), the flow will be retarded due to both the frictional forces and the pressure forces. This could cause the flow near the wall to reverse its direction and cause separation. Separation takes place where the wall shear stress is zero i.e where the velocity gradient is zero (Krause, 2005). Figure 3.5 shows a schematic picture of the event. Separation often leads to the creation of vorticies and to re-circulation of the flow in the negative x-direction of the separation point.

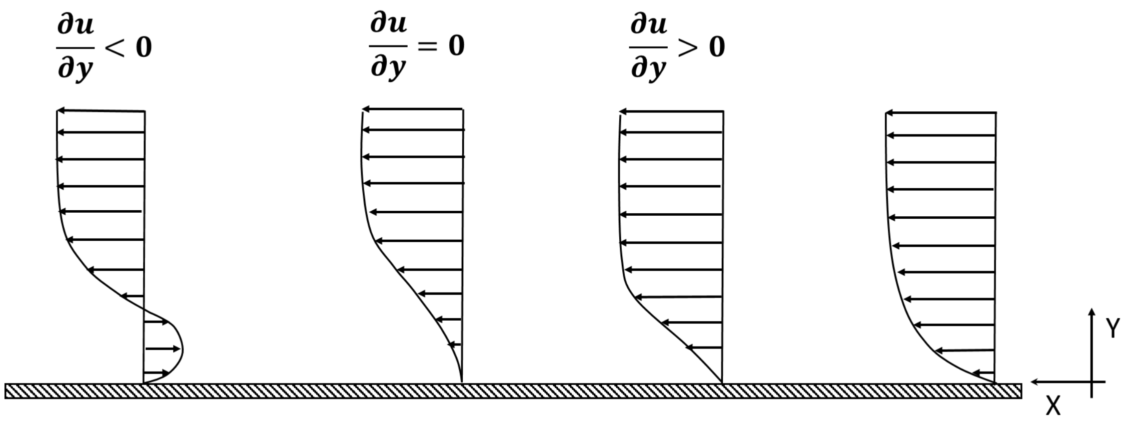

Figure 3.5: Positive pressure gradient effects on boundary layer flow.

One way of analysing the flow on a surface is to look at the wall shear stress vectors, since the direction of the wall shear stress is directly coupled to the flow direction as described in Equation 3.8 (Ferziger and Peric, 2002).

$$\tau_\omega(x,y) = \mu \frac{dV}{z}\bigg|_{z=0} \tag{3.8}$$

Where x and y represent coordinates on the surface, τ_ω is the wall shear stress, μ is the dynamic viscosity, V is the velocity and z the distance to the wall

By defining so called limiting streamlines (or skin friction lines) which are tangential to the wall shear stress vector on the entire surface it is possible to identify areas where separation occurs. The lines must satisfy Equation 3.9 (Yates and Fearn, 1988).

$$\frac{dy}{dx} = \frac{\tau_{\omega,y}}{\tau_{\omega,x}} \tag{3.9}$$

According to Onera (2011) a separation line is defined as a skin friction line that goes through a "saddle point" and depending on the direction of the flow either separation or attachment occurs. To avoid separation of flow it is thus desirable to have limiting streamlines that goes smoothly across the whole surface. Figure 3.6 shows how separation can be identified by looking at the limiting streamlines on a foil.

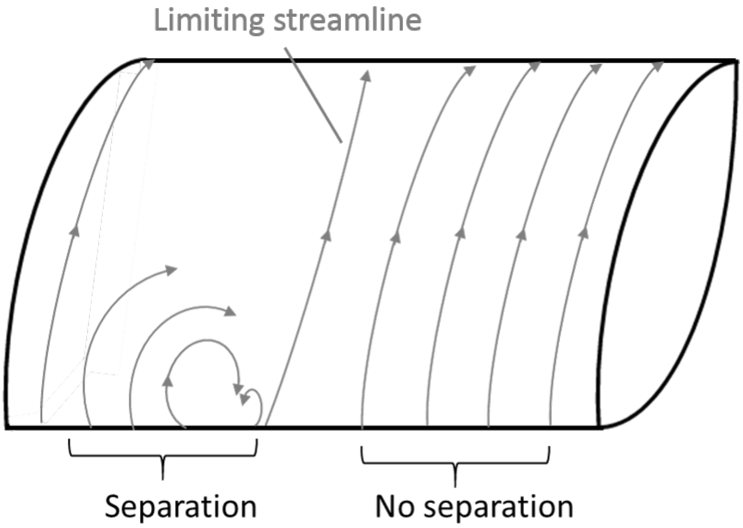

Figure 3.6: Sketch of limiting streamlines over a foil.

3.3 Impeller properties

There are four definitions that are important for this project regarding an impeller blade. The first two are leading and trailing edge, which refers to the two edges of the impeller blade when looking at an cross section in radial direction from the hub. The leading edge is the edge that "meets" the inflow, i.e. the upstream edge, whereas the trailing edge is located further downstream. The other two definitions are called pressure and suction side. The suction side is located at the side of the impeller blade that has its normal direction towards the inflow. This side is dominated by a low pressure gradient, creating a suction of the flow. The opposite side is then called pressure side, where the high pressure instead helps to accelerate the flow further downstream. Figure 3.7 illustrates the four definitions (Dyne and Bark, 2005).

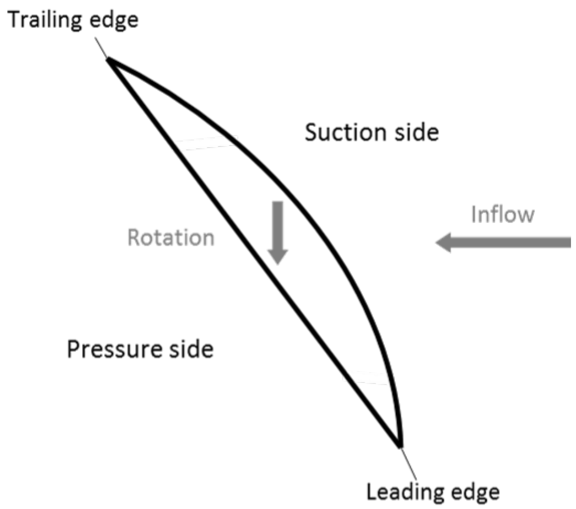

Figure 3.7: Definition of pressure and suction side as well as leading and trailing edge of a propeller. Seen in radial direction of an impeller blade.

3.3.1 Tip clearance

Tip clearance is an important factor when designing an impeller. The tip clearance, h, is defined as the distance between the tip of the impeller blades to the channel wall which the impeller rotates in. Tip clearance is often expressed in millimetres but can also be expressed in percentage of the impeller diameter (Moon-Chan and Ho-Hwan, 2005).

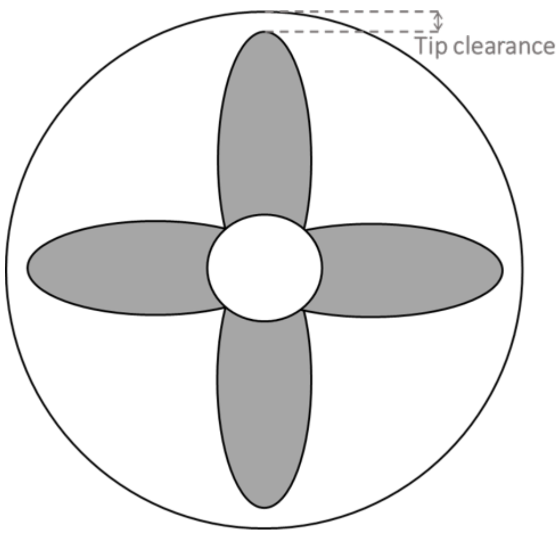

Figure 3.8: Definition of tip clearance of an impeller.

Tip clearances can cause two different effects on the flow in the region between casing and impeller blade tip, Tip Leakage and Tip Leakage Vortex (TLV). The two effects are caused by a too high pressure gradient between the suction and pressure sides of the impeller which makes some flow. The pressure gradient will push some flow upstream of pressure side as in Figure 3.9. When the flow re-enters suction side a vortex can be generated, hence the name TLV. This effect can cause large drops in efficiency and in worst case could cause a blockage of the inflow to the impeller (Wu et al., 2012).

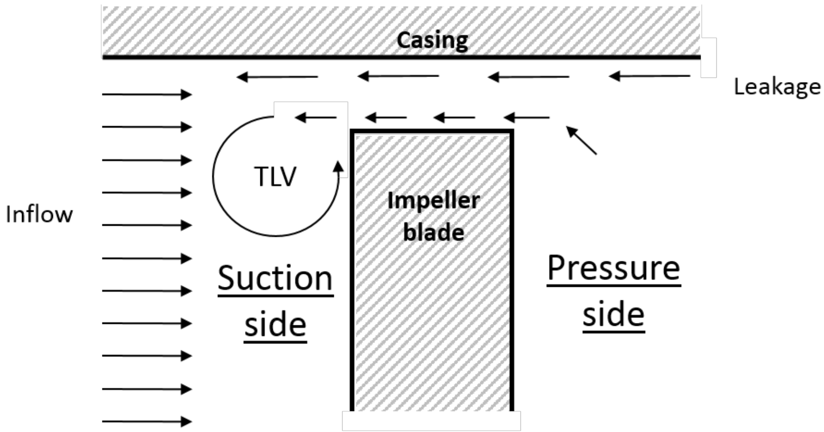

Figure 3.9: Definition of tip leakage and tip leakage vortex.

3.3.2 Cavitation

Cavitation will occur if the local pressure drops below the vapour pressure of the fluid. This will typically occur at the suction side of the impeller blade where sudden pressure drops can occur. Extensive cavitation will lead to an overall decrease in efficiency, increased noise and vibration and possibly damages to the impeller blades (Dyne and Bark, 2005).

It is therefore important to predict under which conditions cavitation can occur and to what extent. The cavitation number σ is described in Equation 3.10. Lower cavitation number means increased risk of cavitation. p is the local pressure, p_v is the vapour pressure and V is the velocity of the flow. Typical vapour pressure for water at 15°C is below 1 700 Pa (Dyne and Bark, 2005).

$$\sigma = \frac{p - p_v}{\frac{1}{2}\rho V^2} \tag{3.10}$$

There are a five different types of cavitation with their own characteristics that are important in this project. A graphic description of the different types is shown in Figure 3.10 followed by a short description of each cavitation type.

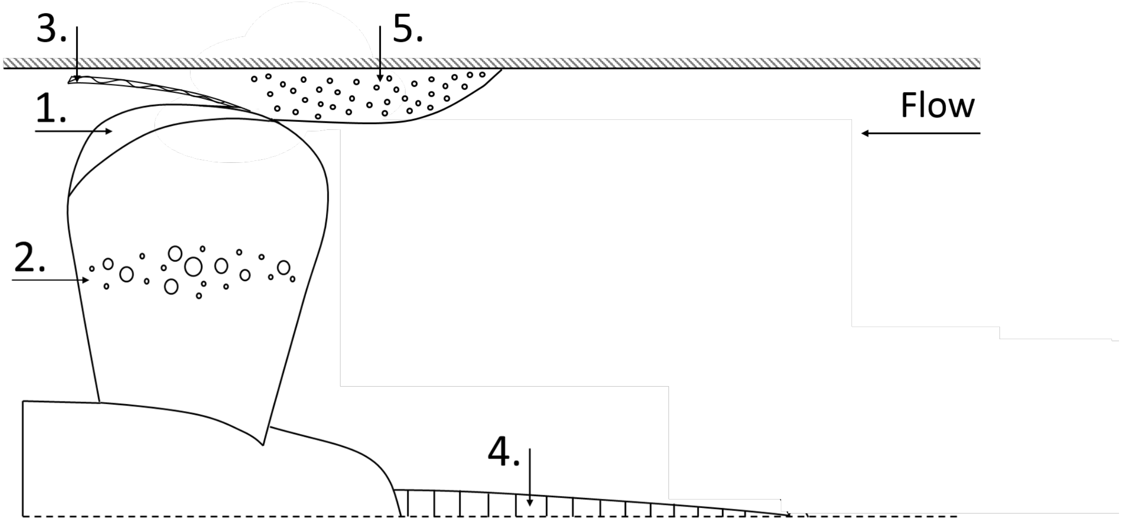

Figure 3.10: Different cavitation types.

1. Sheet Cavitation
Sheet cavitation develops on the side of the impeller blades, which side (pressure or suction side) is dependent on the angle of attack. It covers a part of the blade (partial cavitation) or the whole blade (super cavitation). Sheet cavitation with origin at the leading edge can be delayed by changing the camber against the angle of attack and blade nose shape. When the sheet cavitation reaches its maximum size it collapses and can create "cloud cavitation" which can be seen as bubbles or a cloud down stream (Dyne and Bark, 2005).

2. Bubble Cavitation
Cavitation bubbles are travelling along the suction side with start downstream from the leading edge or at the middle of the blade. Bubble cavitation can be reduced by increasing the blade area and thus reducing the blade load (Dyne and Bark, 2005).

3. Tip Vortex Cavitation
Tip vortex cavitation is caused by an overflow from the pressure side to the suction side at the blade tip. Centripetal forces inside the tip vortexes causes pressure drops which can lead to cavitation. This cavitation type can be spotted as a helix going downstream of the impeller (Dyne and Bark, 2005).

4. Hub Vortex Cavitation
Hub vortex cavitation occurs because of similar reasons as for tip vortex cavitation and can be reduced by decreasing the load on the blades close to the hub or by changing the hub design (Dyne and Bark, 2005). For a waterjet unit hub vortex can occur both on the impeller as well as on the stator hub.

5. Backflow Cavitation
A waterjet system can in addition to the previously mentioned cavitation types suffer from backflow cavitation. This is an effect of the pressure differences between the pressure side and the suction side, causing leakage in the opposite direction of the flow (Yamamoto and Tsujimoto, 2009) as is described in Section 3.3.1.

For very low cavitation numbers the pump unit can experience a cavitation breakdown which means that the flow rate decreases rapidly due to extensive cavitation which blocks the flow.

3.4 STAR-CCM+ properties

This section aims to provide a brief explanation of the theory behind the software in order to get an understanding of potential sources of error and why the software behaves in a certain way.

3.4.1 Meshing techniques

STAR-CCM+ offers a number of different models to generate meshes. In this project two different mesh types are used: the Advancing Layer mesher and the Prism Layer mesher together with Trimmer mesher.

Prism layer mesher
The flow in the near wall regions will need some extra attention as the mean flow characteristics changes rapidly in this region. It is possible to define a prismatic cell layer near the wall to simulate the boundary layer near the wall. The thickness of the prism layers will have to be defined correspondent to the boundary layer thickness at a certain location. It is important that the boundary layer is correctly defined because the first node should ideally be placed at $y^+ \simeq 1$ and nodes 5-10 up to $y^+ \simeq 20$ (Davidsson, 1997).

The following expressions for estimating the boundary layer thickness are gathered from White (2011). Assuming that the whole boundary layer can be estimated using the logarithmic relationship described by Equation (3.11).

Log-law:

$$\frac{u}{u^*} = \frac{1}{\kappa} ln \frac{yu^*}{\nu} + B \tag{3.11}$$

Friction velocity:

$$u^* = \sqrt{\frac{\tau_w}{\rho}} \tag{3.12}$$

With dimensionless constants κ=0.41 and B=5.0.

Reynolds number, here x is the characteristic length, U the mean flow velocity and ν the kinematic viscosity:

$$Re = \frac{Ux}{\nu} \tag{3.13}$$

Estimation of boundary layer thickness:

$$\delta = \frac{0.16x}{Re^{1/7}} \tag{3.14}$$

Skin friction:

$$c_f = \frac{0.027}{Re^{1/7}} \tag{3.15}$$

Wall shear stress:

$$\tau_{w,turb} = \frac{0.0135\mu^{1/7}\rho^{6/7}U^{13/7}}{x^{1/7}} \tag{3.16}$$

Estimation of y^+:

$$y^+ = \frac{yu^*}{\nu} \tag{3.17}$$

Trimmed mesher
The trimmed mesher is an efficient method applicable on many different mesh situations. It creates an hexahedral mesh from a template mesh and then trims the mesh with respect to the defined surfaces. It also offers the possibility to perform parallel meshing of several regions (Siemens PLM Software, 2017).

Advancing layer mesher
The advancing layer mesher creates a prismatic cell layer on the surfaces, this layer is advanced into a volume and then polyhedral cells fills the remaining core volume. The result is more uniform cell layers in comparison to the trimmed mesher. The advancing layer mesher provides good meshes for complex geometries as it controls the thickness of the first layer and thus the y^+ value here, which is not the case for the trimmed mesher (Siemens PLM Software, 2017).

Mesh quality
The mesh quality is checked by diagnosing the volume change between adjacent cells. Too large changes in volume between cells could cause a poor solution. It is suggested that a volume change ratio of 0.01 or smaller gives a poor mesh, where a ratio of 1.0 describes that the cell is equal or larger than its neighbouring cells (Siemens PLM Software, 2017). It is thus desirable to have 100% of the cells in the range between 1.0-0.1 and as few cells as possible in the ranges between 0.1-0.01 and 0.01-0.001. Acceptable values are around 95% and upwards when it comes to the 1.0-0.1 range.

Mesh quality can also be analysed by the y^+ values on the surface as described in this section. Having $y^+>1$ on the surface means that the boundary layer will not be captured in a good manor and a refinement of the mesh needs to be done. Moreover, the mesh quality can also be investigated through the Courant number as is described in Section 3.4.3

3.4.2 Turbulence model

As stated in Section 1.5, the only turbulence model to be used in this project is the $k-\omega$ SST model by Menter (1993). The model is an alteration of the $k-\omega$ model first presented by Wilcox and aims give results without Wilcox's model's dependency of arbitrary free stream values. Menter's model is exactly the same as Wilcox's in the inner parts of the boundary layer but gradually changes into the standard $k-\epsilon$ model for higher y^+ values. The term *SST* is an abbreviation of "Shear Stress Transport" and implies that the model takes into account the transport of principal turbulent stresses in adverse gradient boundary layers. Due to these alterations from the standard $k-\omega$ model, Menter's model is suitable for a number of different flows such as transonic flows and airfoil flows (Fluent Inc., 2006). The turbulence model is also widely used when modelling waterjets.

The governing equations of the $k-\omega$ SST two equation turbulence model are the following (Menter, 1993):

Turbulent kinetic energy:

$$\frac{\partial k}{\partial t} + V_j \frac{\partial k}{\partial x_j} = \frac{1}{\rho} P_k - \beta^* k\omega + \frac{\partial}{\partial x_j}\left[(\nu + \sigma_k \nu_\tau)\frac{\partial \omega}{\partial x_j}\right]$$

Specific dissipation rate:

$$\frac{\partial \omega}{\partial t} + V_j \frac{\partial \omega}{\partial x_j} = \frac{\gamma}{\nu_\tau \rho} P_k - \beta\omega^2 + \frac{\partial}{\partial x_j}\left[(\nu + \sigma_\omega \nu_\tau)\frac{\partial \omega}{\partial x_j}\right] + 2(1-F_1)\sigma_{\omega 2}\frac{1}{\omega}\frac{\partial k}{\partial x_j}\frac{\partial \omega}{\partial x_j}$$

Kinematic eddy viscosity:

$$\nu_\tau = \frac{a_1 k}{\max(a_1\omega, \Omega F_2)}$$

Relations:

$$F_1 = \tanh\left[\left(\min\left[\max\left(\tfrac{\sqrt{k}}{\beta^*\omega y}, \tfrac{500\nu}{y^2\omega}\right), \tfrac{4\rho\sigma_{\omega 2}}{CD_{k\omega}y^2}\right]\right)^4\right]$$

$$F_2 = \tanh\left[\left(\max\left[\tfrac{2\sqrt{k}}{\beta^*\omega y}, \tfrac{500\nu}{y^2\omega}\right]\right)^2\right], \quad P_k = \tau_{ij}\tfrac{\partial u_i}{\partial x_j}$$

$$CD_{k\omega} = \max\left(2\rho\sigma_{\omega 2}\tfrac{1}{\omega}\tfrac{\partial k}{\partial x_j}\tfrac{\partial \omega}{\partial x_j}, 10^{-20}\right), \quad \phi = F_1\phi_1 + (1-F_1)\phi_2$$

Coefficients:

$$\beta_1 = 0.0750, \quad \sigma_{k1} = 0.85, \quad \sigma_{\omega 1} = 0.500, \quad \gamma_1 = \tfrac{\beta_1}{\beta^*} - \tfrac{\sigma_{\omega 1}\kappa^2}{\sqrt{\beta^*}}, \quad \beta^* = 0.09, \quad \kappa = 0.41$$
$$\beta_2 = 0.0828, \quad \sigma_{k2} = 1.00, \quad \sigma_{\omega 2} = 0.856, \quad \gamma_2 = \tfrac{\beta_2}{\beta^*} - \tfrac{\sigma_{\omega 2}\kappa^2}{\sqrt{\beta^*}}, \quad a_1 = 0.31$$

Boundary conditions:

$$\omega = 10\frac{6\nu}{\beta_1(\Delta y)^2} \quad \text{at} \quad y = 0$$

3.4.3 Courant number

The Courant number is an important parameter to consider when a transient solution is used, this in order to avoid convergence rate problems of the solution. Briefly explained, the Courant number is a relationship between the time step length, the local velocity and the cell size to describe how information propagates between two adjacent cells. The definition of the Courant number (CFL) can be seen in Equation 3.18 (Ferziger and Peric, 2002).

$$CFL = \frac{V\Delta t}{\Delta x} \tag{3.18}$$

The Courant number should be less than one to ensure that the information propagates from one cell to an adjacent cell within one time step. The Courant number can be controlled by adjusting the time-step and/or the cell size. It is possible to use Courant numbers over one but with the risk of having a diverging solution (Ferziger and Peric, 2002).

By using the "Convective CFL Time Step Control", STAR-CCM+ can automatically control the time step according to specified input parameters, the mean CFL number and the target CFL number.

3.5 Main particulars of the Wakejet

The main particulars of the Wakejet board and its waterjet unit are shown in Tables 3.1 and 3.2.

Table 3.1: Main particulars of the Wakejet board (Radinn AB, 2016) (Radinn AB, 2017).

Length, L	1900 mm
Beam, B	800 mm
Draught, T	180 mm
Lightship weight	53.5 kg
Rider weight	75-95 kg
Centre of gravity of board	920 mm forward of aft
Maximum speed	25 knots
Number of Intake grills	2
Thrust	890 N

Table 3.2: Main particulars of the Wakejet waterjet (Radinn AB, 2017).

Diameter of casing, D_1	90 mm
Diameter of outlet, D_2	50 mm
Diameter of impeller shaft	12 mm
Impeller	
Number of blades	4
Thickness of blades	2.5 mm
Diameter of blades, D_R	89 mm
Tip clearance, h	1 mm
Operational angular velocity, Ω	680.7 rad/s (6500rpm)
Operational tip speed, U_{tip}	30.29 m/s
Stator	
Number of blades	6

4 Methodology

This section provides a more thorough description of the methodology used in this project compared to Section 1.4. Preparation of CAD-model and set-up of three different CFD simulations in STAR-CCM+ is explained in detail. One CFD set-up is for the whole Wakejet with free surface whereas the two other are for waterjet pumps only, one for the Wakejet waterjet unit and one for the AxWJ-2 validation pump from John Hopkins University. Detailed descriptions of the set-ups to investigate the different waterjet pumps are presented.

4.1 Preparation of CAD geometry

Radinn provided a three dimensional CAD model of the Wakejet. In order to use the model for CFD simulations it must be cleaned and simplified in order to get a well functioning mesh. The preparation of the CAD model is done in two different softwares: CATIA V5 and Rhinoceros 5. CATIA is used to assemble all parts and to make sure that there are no small gaps in between them. Parts which are not necessary to perform the CFD calculations (i.e. parts inside the board such as the battery pack and motor) are also deleted here. Later, Rhinoceros is used to fill holes, such as the screw holes on the nozzle, and trim edges so that all parts are smooth, solid, surfaces. All of these simplifications are performed to reduce the number of cells and thus the computational time as well as to generate a model that is water tight.

The board and the waterjet are prepared independently and then assembled in STAR CCM+. This is because the waterjet will have moving parts that will be defined as different regions in STAR-CCM+.

Examples of the preparation of the CAD model are shown in Figures 4.1 and 4.2.

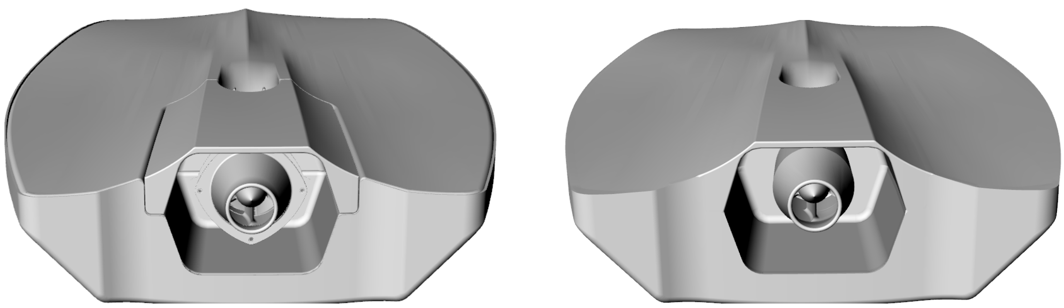

(a) Original model of the Wakejet. **(b)** Prepared model of the Wakejet.

Figure 4.1: Before and after preparation of the CAD model, seen upside down from the aft.

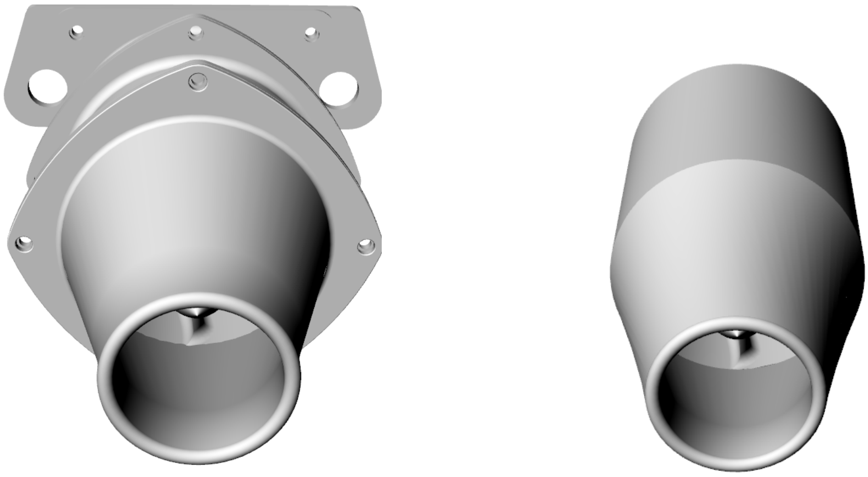

(a) Original model of the waterjet unit. **(b)** Prepared model of the waterjet.

Figure 4.2: Before and after preparation of the waterjet CAD model, seen upside down from the aft.

4.1.1 Repairing the pump

The provided model had parts of the impeller and stator that were orthogonal to the flow. This would lead to blockage and separation of the flow inside the pump unit. In order to make the blades smooth and to avoid disturbances in the flow some additions are made to the impeller, stator and stator cone according to Figure 4.3. The addition to the impeller is 3 mm, the addition to the stator is 3.9 mm at the top and 1.2 mm at the bottom. The addition to the cone is 4.1 mm.

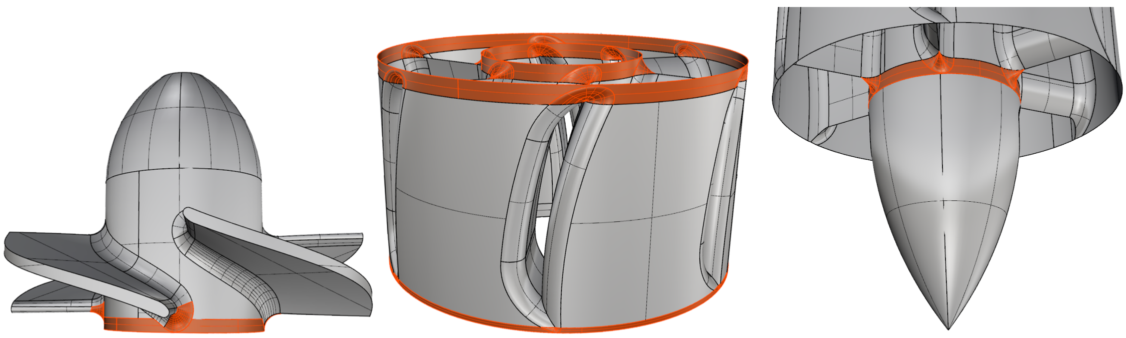

(a) Impeller. **(b)** Stator. **(c)** Stator cone.

Figure 4.3: Additions made to the impeller, stator and stator cone showed in orange.

In the physical product there is a gap between the impeller and the stator, this gap is also closed with this remodelling of the components. However, it is important to remember that any change to the geometry will lead to small inaccuracies when comparing the modelled Wakejet to the real world.

4.2 Set-up of Wakejet simulation

This section presents the work flow in STAR-CCM+ and main particulars of domain size, mesh size and number of cells used.

4.2.1 Setting up the domain

The domain size is chosen according to recommendations from the 26^{th} ITTC (2011). The inlet boundaries should be placed 1-2 L away from the Wakejet and the outlet boundary 3-5 L downstream. This is to reduce the risk of reflection problems from the boundaries. L in this case is the board length of 1.9 meter. The domain size for this setup is therefore created according to Figure 4.4.

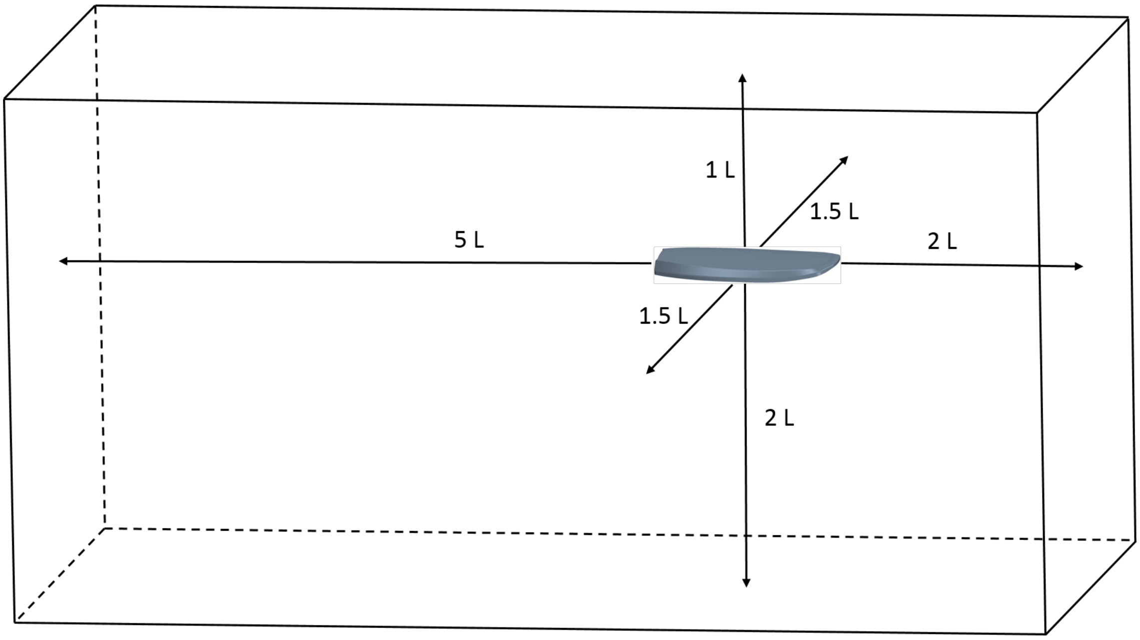

Figure 4.4: Domain size.

The boundaries conditions of the domain are defined as pressure outlet at the face downstream of the Wakejet and velocity inlet at all other faces of the domain.

4.2.2 Splitting the geometry

Since a waterjet system is complex with many different types of geometrical features, a big focus will be on the stator and impeller with regards to creating a well functioning mesh.

The entire Wakejet is split into three regions. One region includes the stator and outlet of the waterjet channel whilst another region includes the impeller and the surrounding channel. The final region includes all other parts, i.e. the computational domain, board, impeller shaft and so on. This region will later simply be called "Board region". The boundaries of the domain and the Wakejet are divided and assigned into three regions which can be seen in Figure 4.5.

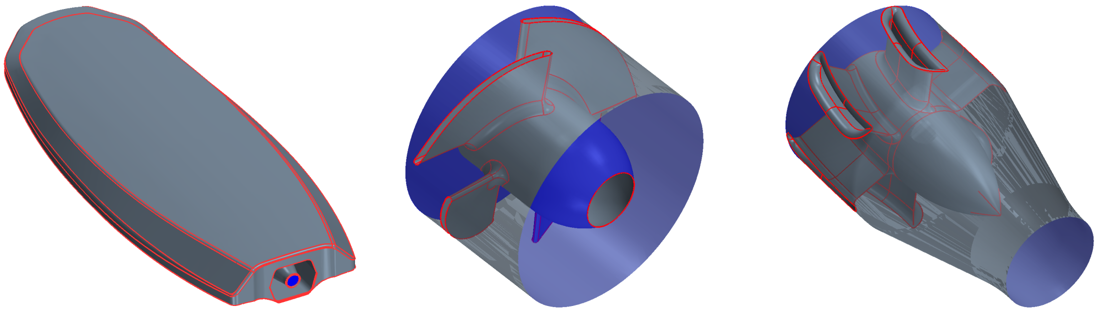

(a) Board region. **(b)** Impeller region. **(c)** Outlet and stator region.

Figure 4.5: Fully prepared Wakejet geometry split into three regions. Red lines show featured curves and blue surfaces show intersections between regions.

Boundary conditions can now be assigned to each region separately. Since the board region includes the computational domain, inlet and outlet conditions are set where they apply. The blue parts in Figure 4.5 shows another type of boundary: intersections. Intersections are set where the three regions intersect with each other. This will enable the water to flow from one region to another by interpolation of values on the boundary cells.

4.2.3 Meshing

The three regions are now meshed separately, where the board region uses prism layer mesher, surface remesher and trimmer mesh models. The two other regions on the other hand use surface remesher and advancing layer mesher which generate a polyhedral volume mesh. An advancing layer mesh is better suited for complex geometries such as the stator an impeller blades, which is why this type of mesh is used in these regions.

Further on, in order to mesh sharp edges of the geometry "feature curves" are defined in the surface repair tool in STAR-CCM+. Feature curves makes it possible to apply specific mesh properties on the chosen curves. The chosen feature curves are seen as red curves in Figure 4.5.

The meshing of the different regions is done using the values presented in Tables A.1 and A.2 (Appendix A.1).

The generated volume meshes on the three regions can be viewed in Figure 4.6.

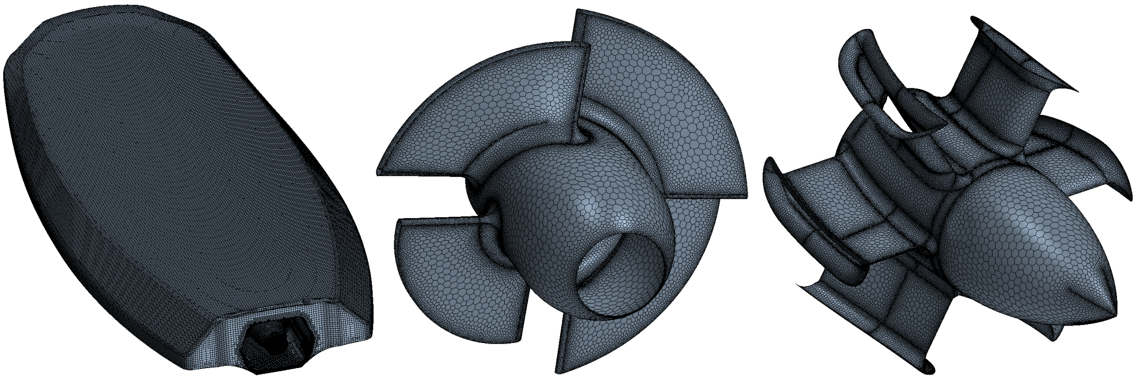

(a) Board region. **(b)** Impeller region. **(c)** Outlet and stator region.

Figure 4.6: Volume meshes of the three regions of the Wakejet.

Apart from the refinements performed on specific surfaces and feature edges, some further refinements in the computational domain are needed. The domain is refined through six geometrical shapes. Firstly, one rectangular shape is created at the free surface so that the wave pattern can be predicted in a good manor, this refinement is rather big so that the board can sink freely and still have the free surface inside the refinement. One triangular shape is created at the free surface to refine the wake created by the board and one cylindrical shape is created around at aft of the waterjet to capture the jet stream coming out of the waterjet unit. Lastly three cubic shapes are created, the largest captures the area surrounding the Wakejet, another refines the volume very close to the Wakejet and the third is located in the intake area to the waterjet unit. Table A.3 (Appendix A.1) shows the properties of each geometrical refinement of the domain.

The final generated volume mesh, including domain refinements, consists of approximately 18 million cells and can be seen in Figure 4.7. Exact number of cells as well as mesh quality can be seen in Appendix A.10.

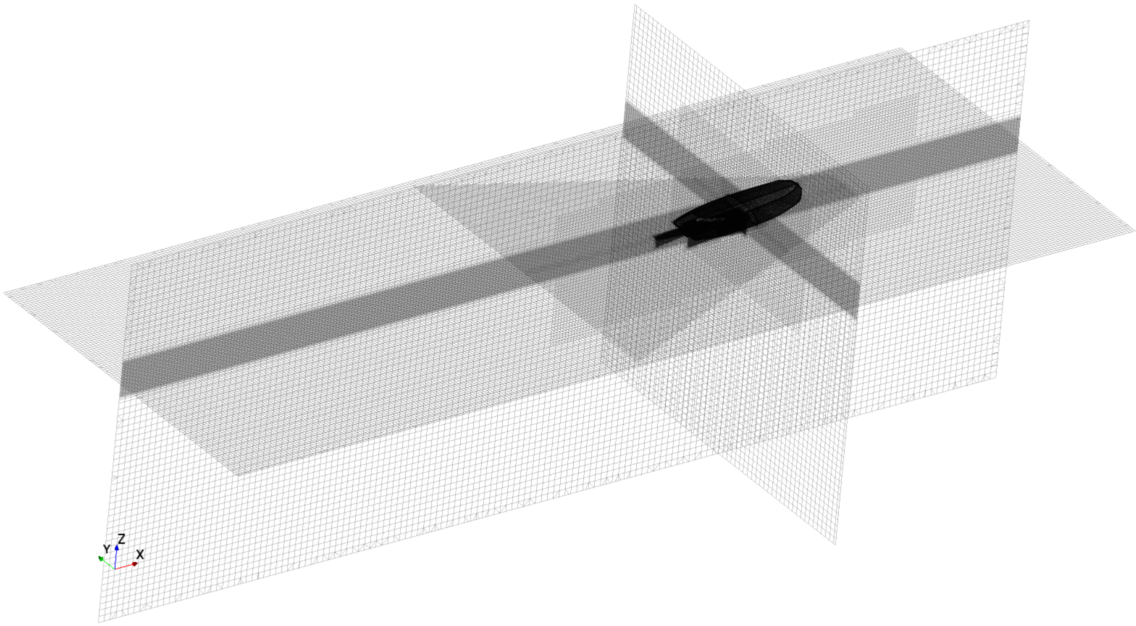

Figure 4.7: Volume mesh over the whole domain, including refinements.

4.2.4 Computational models

The next step after a mesh is generated is to set-up the physical conditions of the simulation. The computational models, called physical models in STAR-CCM+, used in the simulations can be seen in Table A.4 (Appendix A.2).

Since the computational domain includes both volumes under and over the board the Eulerian Multiphase model is defined. Two phases are created, one for the water and one for the air. Both phases are assumed to have constant density. The VOF multiphase model is used to simulate the phase interactions such as the interaction between the free water surface and the surrounding. It could also be used to simulate changes of state such as cavitation by adding a vapour phase and defining a phase interaction. The VOF model uses the HRIC (High Resolution Interface Capturing) convection discretization scheme to capture the convective transport of the different phases and to ensure that the phases are immiscible and separated by a sharp interface (Siemens PLM Software, 2017).

The VOF wave model is commonly used in the marine industry to capture the behaviour of the surface gravity waves that is created by the vessel and thus the interaction between the water and the air above the surface. This thesis will only focus on the flat wave i.e a initially calm water surface. One single flat VOF wave is created with current and wind speed set as constant on the Wakejet speed that is simulated (5, 10, 15, 20 or 25 kn) in negative x-direction.

When it comes to setting up the initial conditions, the pressure is set to hydrostatic pressure of the flat VOF wave created earlier. The velocity is set as velocity of the same wave. The volume fraction is set as a composite of the fractions of water and air. The volume fractions are functions of the water and air volume fractions of the VOF wave. The same initial conditions are also applied on the inlet and outlet boundaries. The VOF wave Damping option is enabled and set to a length of 0.3m on the inlet and outlet boundaries in order to minimise reflections of the flow.

4.2.5 Pump modelling

There are different ways to simulate rotation of certain regions. One way is to assign a wall-relative rotation to specific boundaries in a region. This is applied on the impeller shaft in the Board region, which rotates at the same Revolutions Per Minute (RPM) as the impeller. Another method is however used for the impeller. Instead, the whole Impeller region gets a rotation about its axial direction. This can be done with two different techniques: Moving Reference Frame (MRF) and Rigid Body Motion (RBM). Important to remember is that the non-rotating channel surrounding the impeller also is included in this region. This is fixed by applying a negative wall-relative rotation to this boundary to counteract the rotation.

Moving Reference Frame
The simplest method of modelling rotation to a whole region is MRF. Here the impeller is stationary and source terms are added to the moment equations to represent the rotating motion (Bulten and Esch, 2007). Important to note is that the geometry is not physically moved in the model.

The MRF technique is less accurate than the RBM technique as it will not account for the unsteady flow interactions within the system (Siemens PLM Software, 2017). Effects such as the relative position between impeller blade and stator will not be taken into account. The MRF technique itself is not dependent on the time step in order to converge which makes it possible to have longer time steps compared to RBM. This makes the technique cheaper than RBM when it comes to computational time. In this project a time step of 0.025s is used in MRF simulations until convergence is achieved.

Rigid Body Motion
Another rotation technique that is available in STAR-CCM+ is called Rigid Body Motion which is more accurate compared to the MRF. On the other hand it is a much more expensive method. In the RBM the whole mesh of the region will physically rotate, as it does in reality. This method is time dependent(unsteady), making the chosen time-step an important parameter to obtain a converging solution. Siemens PLM Software (2017) recommends a time-step that gives a rotation of 1 degree between each time step. For a rotational speed of 6500 RPM this corresponds to a time step of $25.6*10^{-6}$s.

Due to the short time step for a RBM simulation, convergence of all parameters would be very expensive to achieve. Instead, RBM simulations will continue to run on the MRF simulations that already have converged. Because of that, only two revolutions of the (720 additional time steps) impeller are simulated to capture the unsteady behaviour in the impeller.

4.2.6 Wakejet motions

The Wakejet is initially fixed in its position relative to the free water surface. This is done to first ensure that the simulations of the waterjet unit are running as they should and to stabilise the solution. Later translation in z-direction (sinkage) will be allowed to find the equilibrium position at different velocities.

Only sinkage will be enabled because the trim (rotation about the y-axis) and roll (rotation about the x-axis) of the Wakejet are heavily influenced by the rider. The rider controls the motions of the Wakejet by changing the centre of gravity. It can be concluded from real life observation that the centre of gravity needs to be moved forward when the Wakejet reaches planing-mode and thus reduce the running trim angle in order to stabilise the ride. To turn the Wakejet the centre of gravity needs to be moved to one of the sides as the Wakejet is not equipped with any other steering device. The Wakejet will instead be given a fixed trim angle in STAR-CCM+.

The free sinkage simulation is set-up by creating a "DFBI Rotation and Translation motion" in Star-CCM+. This will create a 6DOF-body that is going to be used in the simulations. The parameters used in the set-up can be seen in Table A.5. Radinn AB (2017) have stated that the riders usually weighs between 75-95 kg. Due to lack of time simulations are only performed for a rider weighing 75kg. Furthermore, the centre of mass is approximated to be roughly in the centre of the board. Since only free sinkage is allowed, the parameter that is important is the total mass of the Wakejet and rider whereas the exact position of the centre of gravity is insignificant. Moreover, the moment of inertia is defined through Equation 3.1 even though it will not have an impact of the results due to the lack of free trim. A more exact value on the moment of inertia could however help to stabilise the solution.

In order to simulate the rotation of the impeller together with the sinkage of the board a DFBI superposed rotation is created and applied to the impeller region. The superposed rotation can use both MRF and RBM as in Section 4.2.5.

The last two parameters that are set in the 6DOF-body is Release and Ramp time. Release time is the physical time that the motion of the body begins. According to Siemens PLM Software (2017) this should be set to somewhere between 10-50 time-steps. The ramp time on the other hand is a subsequent ramp up of the motion forces acting on the body, it is recommended that this time is about 10 times the release time to get a converging solution. Having too short release and ramp times could lead to a rapidly diverging solution due to too many physical effects happening at the same time. Table A.5 (Appendix A.2) shows all parameters that are used as input to the 6DOF-body.

In order to perform self-propulsion simulations on the Wakejet the waterline and impeller RPM must be matched to the speed that the Wakejet is moving. Six different speeds are simulated in this project: 5, 10, 15, 20 and 25 knots. For each speed two forces needs to be matched: Lift and Drag. The drag force is defined as the total force acting on the board in x-direction (the direction the board is going). For each speed the waterjet unit must produce enough thrust forward to match the resistance of the board in order to have the board going at a constant speed. A too small thrust compared to the resistance means thus that the impeller needs to rotate at a higher speed and vice versa.

The board also needs to generate enough lift force, i.e. total force acting in z-direction, to match the total weight of the Wakejet and rider. In the self-propulsion tests STAR-CCM+ will heave the board up and down until a lift force matching the weight is achieved. The lift force is also dependent on the trim angle of the board since it affects the volume of water that is displaced and thus generating equal lift according to Archimedes' principle.

4.2.7 Solvers and convergence criteria

Apart from the time-steps, maximum physical time and maximum steps most solver and stopping criteria are set as their default values. The only parameters that are changed are the temporal discretization and the "solver frozen" options on the partitioning and wall distance solvers. The Wall distance solver controls the computation of the wall distance for the 'Exact Wall Distance'-model and the partitioning determines how the domain is partitioned. Solver frozen means that the solution is not updated while iterating.

Important to note is that the inner iterations, i.e. the number of iterations within each time-step, could be increased if the solution diverges. The solver and stopping criteria used for both techniques can be seen in Tables A.6 and A.7 (Appendix A.3) respectively.

4.2.8 Post processing

The simulation is now ready to run, but in order to analyse the results of the simulations a number of post-processing scenes and reports are created.

The wall y^+ is analysed on the impeller blades, impeller shaft, stator and on the intake grills as this is the part of the geometry with the most motions and fluctuations of the flow. The analysis is done by creating an iso-surface on the mentioned surfaces with an upper limit of y^+=2. The Courant number is analysed for all parts of the Wakejet to analyse the mesh quality further and to find potential problems regarding convergence rate. A scene showing a cross section of the whole Wakejet from the side is created to capture all parts of the flow.

A scene showing the volume fraction of water in the domain at a cross section seen from the side of the Wakejet is created so that the risk of water being injected into the waterjet system is visualised. This scene also serves as a way to see if a common numerical error regarding fast going ships with waterjets occurs: water being trapped under the board and thus injected into the waterjet system. This error could affect the resistance of the board as well as the flow behaviour inside the pump since the fluid would not be the same as in reality. If this behaviour indeed does occur a source term sucking air out of the near wall region will be added to the model.

Geometry scenes showing an iso-surface simulating the free surface and jet stream around the board and inside the waterjet is created so that the flow around the hull can be analysed. To study the effects of the intake grills the vorticity is shown together with the velocity vectors at a cross section of the intake seen from the side of the Wakejet both with and without intake grills. Another scene orthogonal to the previous one is created showing the velocity profile upstream of the impeller. Both scenes are created with and without the intake grills to compare the differences. Moreover, an iso-surface showing the areas where the pressure drops below vapour pressure for water at 25°C is created to find areas with risk of cavitation.

Two plots are created, both showing different results as functions of the iteration number. The first plot shows a number of different residuals, i.e. convergence rate, whereas the other shows Lift and Drag forces exerted on the Wakejet. As mentioned in Section 4.2.6, the total drag force should be equal to zero and the lift force should match the weight of the Wakejet and rider for self-propulsion simulations.

4.3 Set up of AxWJ-2 validation simulation

In order to validate results from simulations on the Wakejet waterjet unit an additional study is conducted on the well documented AxWJ-2 axial waterjet pump from the John Hopkins University (Tan et al., 2015) where measured data is available. Table 4.1 shows relevant data for the AxWJ-2 pump. Notable is that the AwXJ-2 has an impeller diameter which is approximately three times larger than that on the Wakejet waterjet. Additionally, simulations on the AxWJ-2 are run at 900 RPM since a substantial amount of measured data is available at this rotational speed.

Table 4.1: Main particulars of the AxWJ-2 pump.

Diameter of casing, D_1	304.26mm
Diameter of outlet, D_2	213.4 mm
Impeller	
Number of blades	6
Diameter of blades, D_R	303.8 mm
Tip clearance, h	0.46 mm
Tip profile chord length, c	274.3 mm
Tip profile axial chord length, c_A	127.4mm
Angular velocity, Ω	94.2 rad/s (900rpm)
Tip speed, U_{tip}	14.3 m/s
Stator	
Number of blades	8

The AxWJ-2 pump tested at the John Hopkins University uses a liquid solution of sodium iodide (NaI) in water (62-63% of weight), the density of this liquid is 1800 kg/m^3, its dynamic viscosity is 0.00198 Pas and its vapour pressure is approximately 1130 Pa in the temperature range of 20°C - 23°C. The vapour pressure of the NaI solution is thus slightly lower than for water at the same temperature.

The AxWJ-2 waterjet are simulated in STAR-CCM+ to match the set-up described by Tan et al. (2015). The simulations on AxWJ-2 in STAR-CCM+ will then be compared to the measured data and to validate the setup technique. Figure 4.8 shows the experimental setup of the AxWJ-2 pump used by Tan et al. (2015).

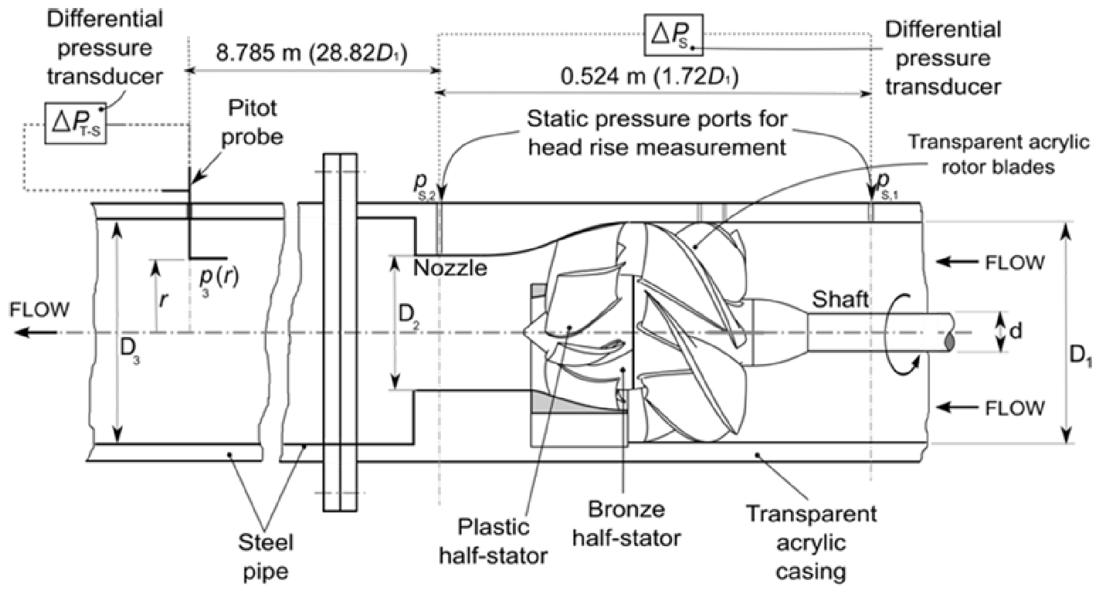

Figure 4.8: Experimental set-up of the AxWJ-2 pump (Tan et al., 2015).

The experimental setup at the John Hopkins University is imitated in STAR-CCM+ according to Figure 4.9. The mean pressure and velocity is measured at one position before and one position after the pump unit in accordance to the experimental set-up ($p_{s,1}$ and $p_{s,2}$ in Figure 4.8). The pressure is measured as the wall surface pressure and the velocity is measured as the surface average of the cross section at each of the two positions. Additionally, Torque and Thrust is also measured on the impeller.

The work flow of generating mesh and setting physical conditions is similar to that for the Wakejet, but with two large differences. Due to the larger size of the AxWJ-2, the mesh values are roughly three times larger than those in Tables A.1 and A.2. Most importantly, this simulation does not use VOF, but only a single fluid being water.

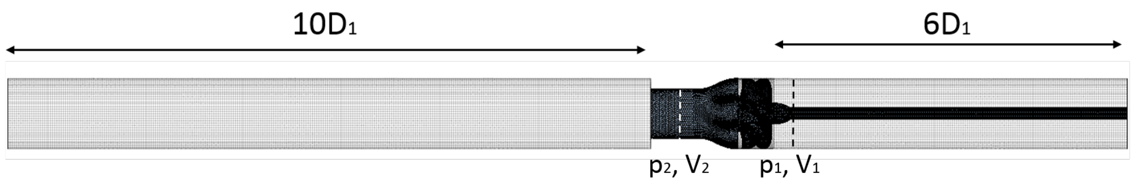

Figure 4.9: Set-up of the AxWJ-2 pump in STAR-CCM+.

The range of the inlet velocity is calculated backwards from Equation 3.5 using the flow rate coefficient, ϕ, from the experimental measurements. This is done so that the results obtained will be in the same range as the measured data. The inlet velocities and corresponding flow rate coefficients ϕ used in STAR-CCM+ can be seen in Table 4.2. Where V_1 is used as the velocity at the inlet boundary. Using Equation 3.4 together with data from simulations, efficiency and head rise curves can be calculated and compared.

Table 4.2: Inlet velocities, V_1, and corresponding flow rate coefficients, ϕ.

V_1, [m/s]	3.539	3.982	4.203	4.424	4.645	4.867	5.088	5.301	5.751
ϕ	0.608	0.684	0.722	0.76	0.798	0.836	0.874	0.912	0.988

4.3.1 Cavitation study

In order to simulate cavitation in STAR-CCM+ a couple of alterations to the set-up explained in Section 4.3 needs to be done. In order to simulate cavitation an additional gas phase is created to represent the vapour that is generated by cavitation. Also, the phase interaction between the liquid phase and the gas phase is defined. The primary phase is set as the liquid and the secondary phase as gas. Initially the simulation contains only the liquid phase and its vapour pressure is defined according to the properties of the liquid (see section 4.3).

It is important that the boundary conditions matches the conditions of reality as the occurrence of cavitation is sensitive to pressure differences. It can be seen at the John Hopkins University that a pressure difference of just two kPa can alter the magnitude of the cavitation on the impeller blades a lot (Chen et al., 2016).

In order to match the cavitation number to the measured data, the static pressure is calculated backwards from the known range of cavitation numbers from (Chen et al., 2016). The calculated pressure is used as the reference pressure in the simulations at the first measuring position. The flow coefficient is kept at a constant number and the reference pressure is changed to alternate the cavitation number according to Equation 3.10.

The cavitation in the simulations can be visualised by creating scenes showing the volume fraction of vapor. Notable is that this can only be done if the conditions of the John Hopkins University are matched sufficiently. If the conditions does not match then then the effects of cavitation in the simulations are visualised by showing areas on the impeller surface where the pressure is below the vapor pressure. This can be used as an indication of when cavitation can occur, assuming that the pressure distribution is correct. The results are then compared to different cases of cavitation for the AxWJ-2 pump.

4.4 Set-up of Wakejet pump simulation

In order to save computational time a simplified waterjet system is created, consisting of only parts belonging to the waterjet system, to simulate the behaviour inside the waterjet. This also makes it possible to conduct a series of different studies on the waterjet system such as cavitation and the effect of different tip clearances using only a small amount of computational time.

The waterjet is simplified to only a cylinder going into the impeller and a cylinder connected to the nozzle at the outlet so that the geometry resembles that of Figure 4.9 as much as possible. Just as with the case of the AxWJ-2, the set-up in STAR-CCM+ is similar to that for the Wakejet but with a single fluid instead of VOF. The geometry is meshed using the same mesh set-up as in Tables A.1 and A.2. The mesh generated for the simplified waterjet unit used on the Wakejet can be seen in Figure 4.10.

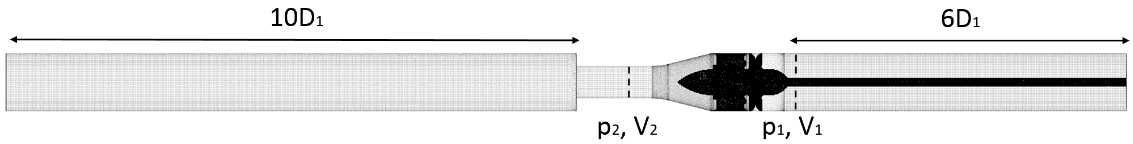

Figure 4.10: Set-up of the simplified Wakejet waterjet unit without intake grills.

Using the simplified waterjet system and the inlet velocities specified in Table 4.3, the efficiency and head rise can be calculated using equations 3.3 and 3.4. Once again, velocity and pressure is measured just before and after the impeller. Torque and Thrust is also measured on the impeller.

4.4.1 Inlet velocity to the impeller

As described in Section 3.2.2, the inflow to the impeller (V_1) will be significantly lower than the free stream velocity (V_s). The inlet velocity is in this case determined by calculating the average velocity on a cross-section inside the waterjet system in a simulation including the whole Wakejet. In that way inlet velocities for board speeds at 5, 10, 15, 20 and 25 knots are decided. Six additional inlet velocities are also simulated to capture the behaviour of the waterjet properly.

Table 4.3 presents the eleven different inlet velocities that are simulated together with flow coefficients as well as corresponding board speed when applicable.

Table 4.3: Simulated inlet velocities, V_1 (m/s), flow coefficient, ϕ, and corresponding Wakejet speeds, V_s.

V_1	0.75	1.5	1.8	2.25	3	3.2	3.75	4.5	5	5.5	6
V_s	-	-	5kn	-	-	10kn	-	15kn	-	20kn	25kn
ϕ	0.059	0.119	0.142	0.178	0.234	0.252	0.30	0.356	0.395	0.434	0.474

4.4.2 Impeller tip clearance study

In the original CAD model both the impeller and impeller casing have a diameter of 90mm, giving the impeller no tip clearance. In real life this will not be favourable since the impeller tip will rotate on the casing resulting in large losses to friction. The actual impeller used on the Wakejet has however a tip clearance of 1mm. Two additional impellers with tip clearances of 0.5mm and 1.5mm are also created so that a study of the effect of tip clearance can be conducted.

4.4.3 Evaluation of simulation technique

Section 4.2.5 thoroughly explains the fact that the RBM technique is more exact compared to the MRF when it comes to modelling rotation of the impeller but also much more expensive. Hence, it is desirable to perform as few RBM simulations as possible and still achieve results that are reasonable. Because of this RBM simulations are only run on the impeller with a tip clearance of 1mm initially. Pump performance curves for both MRF and RBM simulations are generated and compared. If the two techniques show similar results all other simulations will only be performed using MRF.

4.5 Pump studies

This section aims to describe the methods used to evaluate the flow within the waterjet system of both AxWJ-2 and Wakejet waterjet.

Tip Leakage
If the pump has a tip clearance it could face problems with flow going in the opposite direction to the main flow, as described in Section 3.3.1. This is visualised by creating an iso-surface showing these velocities as well as investigating the velocity vectors close to the impeller tip.

Limiting streamlines
Limiting streamlines are created to investigate if there are any areas of separation. This is done by using a software called Tecplot 360 which is able to create limiting streamlines on the impeller and stator parts using exported data of wall shear stress from STAR-CCM+. Areas with separation can be identified by seeing where the wall shear stress is zero. Another indication of separation is areas where the limiting streamlines goes in the opposite direction of the flow.

Streamlines
Streamlines are created over the whole volume to get an image of how the flow enters and behave inside the pump. The streamlines makes it possible to find areas of problem regarding outlet flow and blockage easily.

Swirl
The swirl shows the non axial velocities of the mean flow and is an indication of losses in the system. Cross sections before the impeller, between stator and impeller, after stator and at the nozzle outlet is created. Ideally the stator should cancel the swirl so that the waterjet has an uniform outflow purely in the axial direction. Velocities in non-axial directions should be seen as loss of kinetic energy.

Impeller and stator torque
A way of analysing the stator performance is by looking at the torque of the stator since the stator should counteract the swirl given to the flow by the impeller. The stator torque, T_{stator}, should thus counteract the impeller torque, T, so that $T - T_{stator} = 0$. The impeller and stator torques are thus calculated and plotted against flow rate for both pumps. Having a impeller torque larger than the stator torque indicates that the stator does not work as intended and that swirl is still left in the flow at the outlet.

5 Results

This section summarises the results obtained from simulations and calculations presented in the previous chapters.

5.1 Validation of AxWJ-2 performance

In this section the results obtained from the simulations on the AxWJ-2 pump in STAR-CCM+ and together with measured data by Tan et al. (2015) when possible. The section starts with results to analyse the mesh quality and goes on to show pump performance curves, tip leakage, limiting streamlines and swirl vectors.

5.1.1 Mesh quality

In order to determine whether the chosen wall distance is appropriate, i.e. so that the first node is placed at $y^+ \simeq 1$ (see Section 3.4.1), the wall y^+ values are illustrated on the waterjet surfaces for the highest velocity simulated.

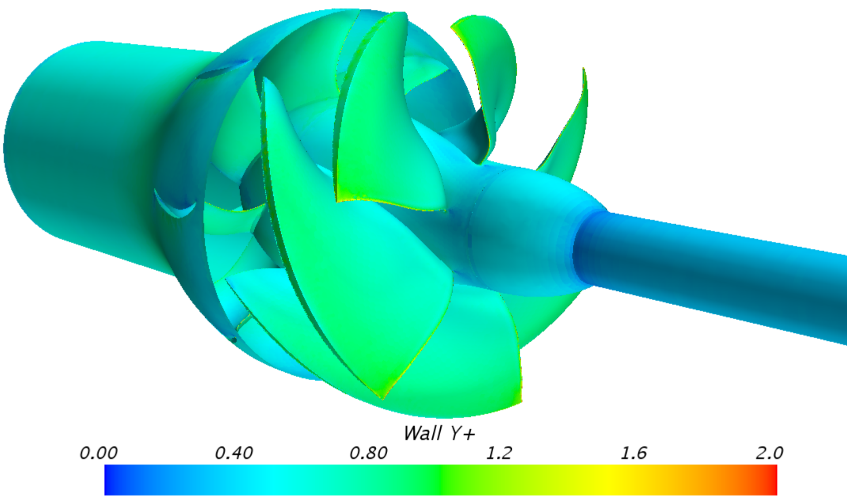

Figure 5.1: y^+ values for the first node on the AxWJ-2 mesh at V_1=5.75 m/s with the impeller rotating at 900 RPM using RBM.

Moreover, the volume change ratio between 1.0-0.1(Appendix A.5) is approximately 96.5% for the Wakejet model.

5.1.2 Pump performance curves

The pump efficiency, η, and the head rise, H, are plotted as functions of the volumetric flow rate, Q, in Figure 5.2. The maximum calculated efficiency is η=89.55% at Q=0.3435 m^3/s with a head rise of 4.963 m. Unfortunately no data on torque is provided from measurements, making it impossible to plot the efficiency curve. The maximum efficiency point is however stated to be 89% at Q=0.3478 m^3/s. Head rise curve from measurements is plotted in Figure 5.2.

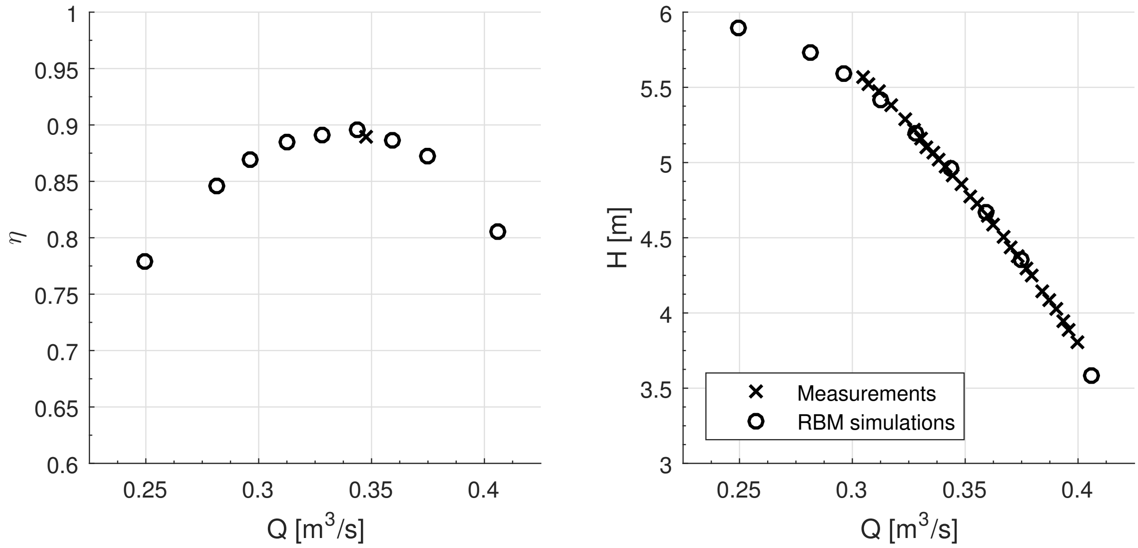

Figure 5.2: Efficiency and head rise over volumetric flow rate for the AxWJ-2 waterjet at 900 RPM using RBM together with the best efficiency point and head rise curve from measurements.

Measurements at the John Hopkins University are plotted together with the calculated flow rate coefficient ϕ and the head rise coefficient ψ. The calculated values of ϕ and ψ are scaled with ϕ_{BEP}=0.76 and ψ_{BEP}=2.46 where BEP is the "Best Efficiency Point" obtained from the measured data. It is clearly shown from Figure 5.3 that the calculated results corresponds well to the measured data.

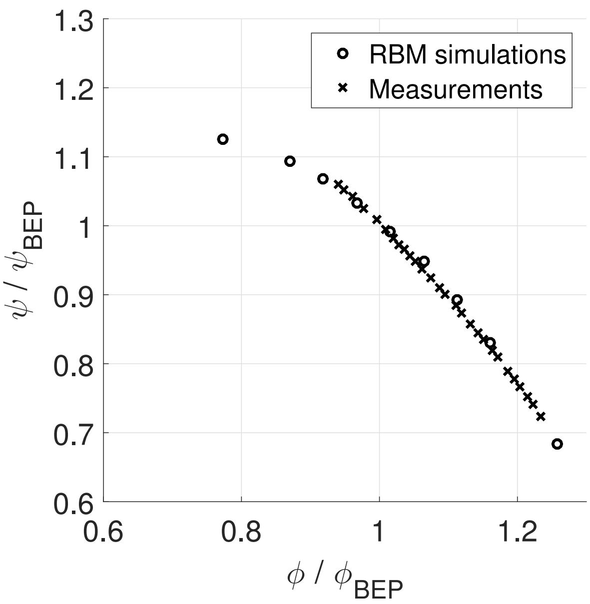

Figure 5.3: Comparison between RBM simulations and test data for the AxWJ-2 waterjet at 900 RPM.

5.1.3 Pump flow

Figure 5.4 shows an iso-surface of flow going in the reversed flow-direction on the impeller for three different inlet speeds. Tip leakage occurs when the iso-surface (blue) is located at impeller blade tips.

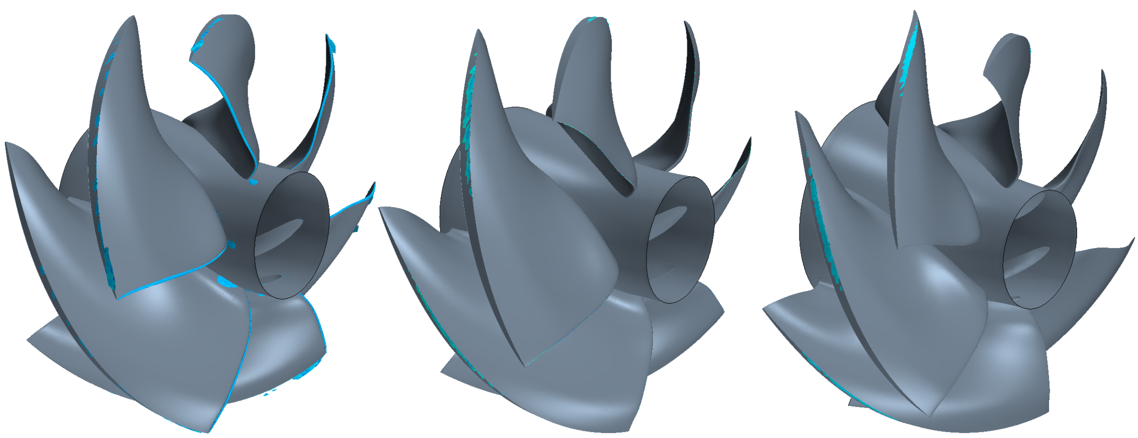

(a) V_1=3.539 m/s. **(b)** V_1=4.867 m/s. **(c)** V_1=5.75 m/s.

Figure 5.4: Illustration of water flowing in the opposite direction of the main flow in the tip clearance region, for impeller going at 900 RPM using RBM.

The limiting streamlines on impeller and stator are shown in Figure 5.5. All streamlines seem to follow the geometry smoothly with few signs of separation except maybe at the leading edges of the stator blades.

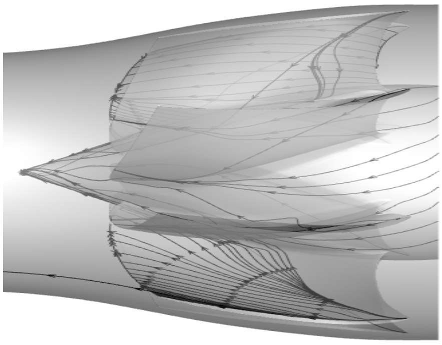

(a) Stator.

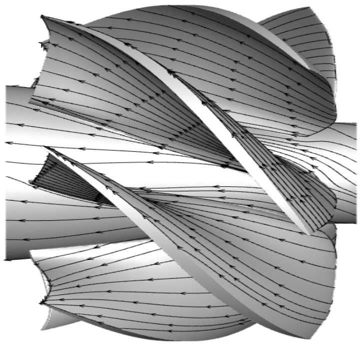

(b) Impeller.

Figure 5.5: Limiting streamlines on the AxWJ-2 waterjet system with an inlet speed of V_1=5.75m/s the impeller rotating at 900 RPM using RBM.

The streamlines in the single fluid volume are shown in Figure 5.6.

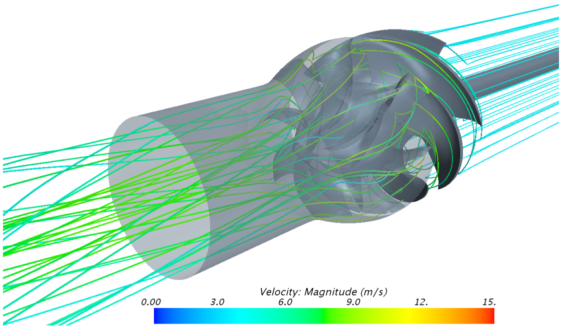

(a) V_1=3.539 m/s.

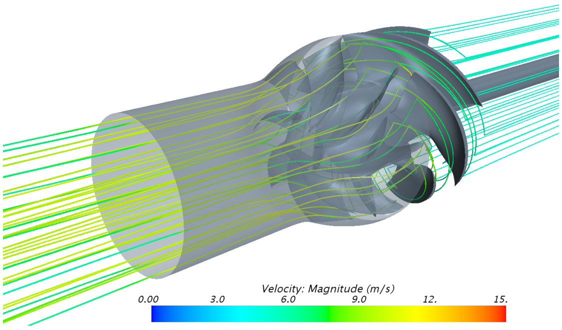

(b) V_1=4.867 m/s.

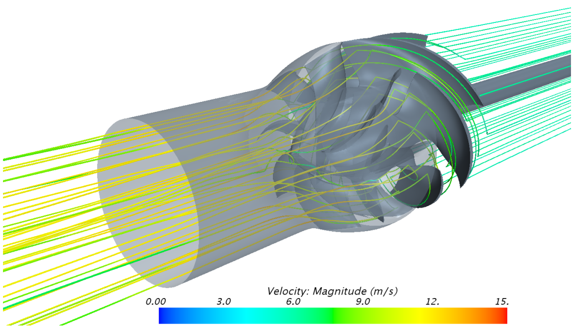

(c) V_1=5.75 m/s.

Figure 5.6: Streamlines in the AxWJ-2 waterjet system at three different inlet speeds with the impeller rotating at 900 RPM using MRF.

Swirl vectors at different positions in the waterjet system are shown in Figure 5.7.

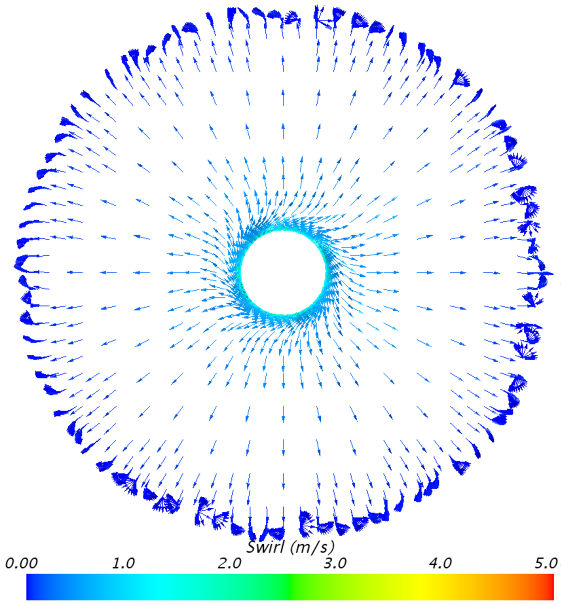

(a) Before impeller.

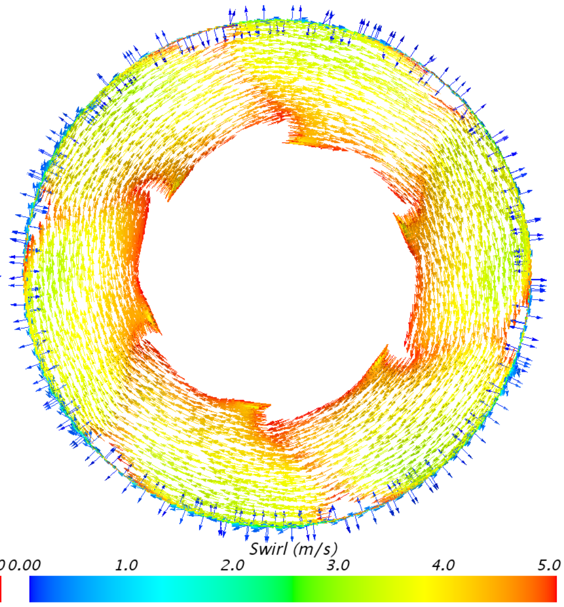

(b) Between stator and impeller.

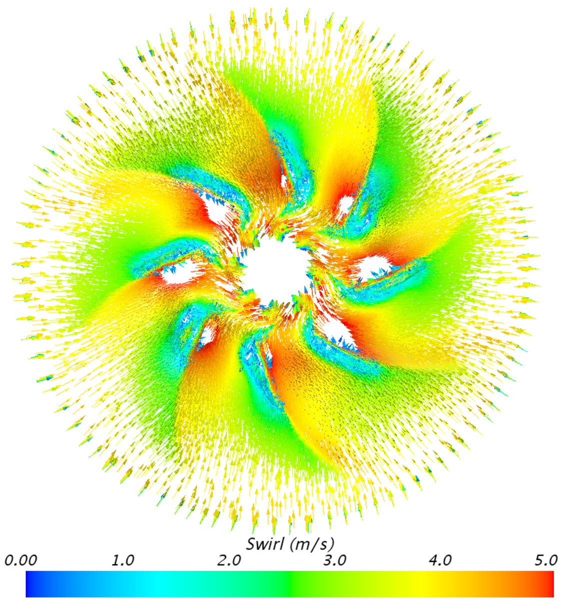

(c) After stator.

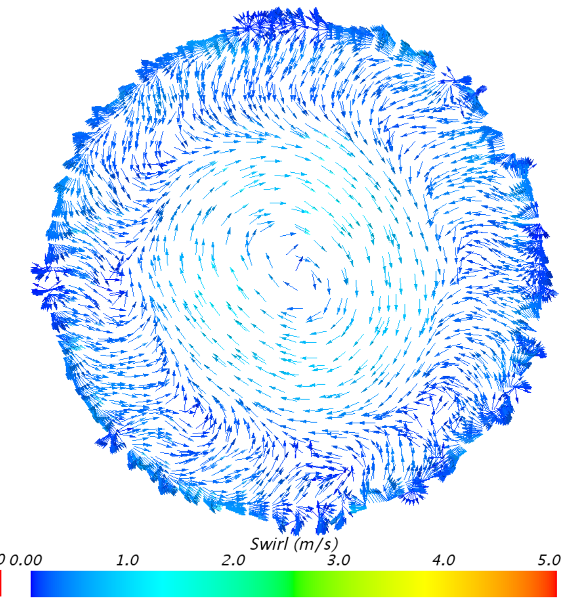

(d) At the outlet.

Figure 5.7: Swirl vectors at four different positions inside the AxWJ-2 waterjet going at 900 RPM using RBM at V_1=5.75m/s.

By looking at Figures 5.6 and 5.7 it becomes clear that the stator does a good job of reducing the swirl of the flow exiting the impeller. Moreover, Figure 5.8 shows that the ratio between impeller and stator torque is close to one, especially at high flow rates, further indicating that the stator is well designed.

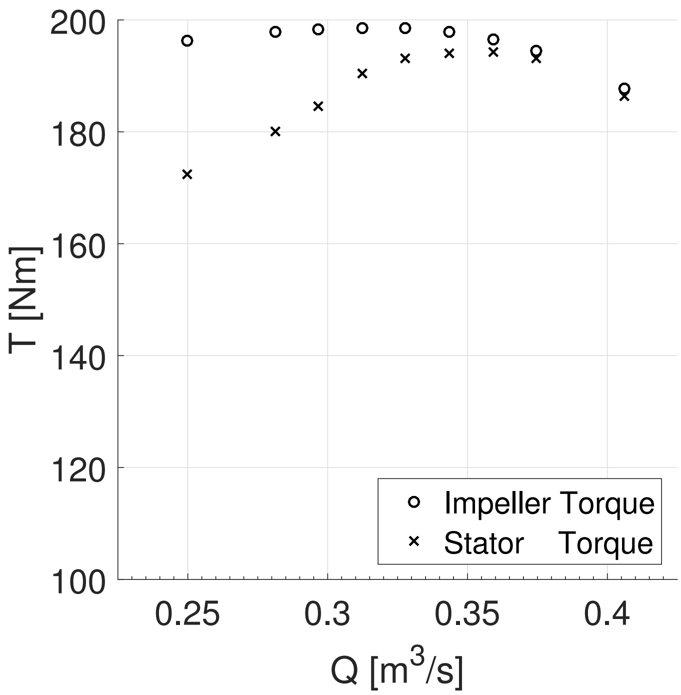

Figure 5.8: Comparison between impeller and stator torque magnitude for the AxWJ-2 waterjet simulated at a fixed RPM of 900 using RBM.

5.1.4 Cavitation

The simulations of the AxWJ-2 are compared to the measured data. The flow rate coefficient ϕ is set to 0.675 initially and the reference pressure is changed. The results are plotted in Figure 5.9.

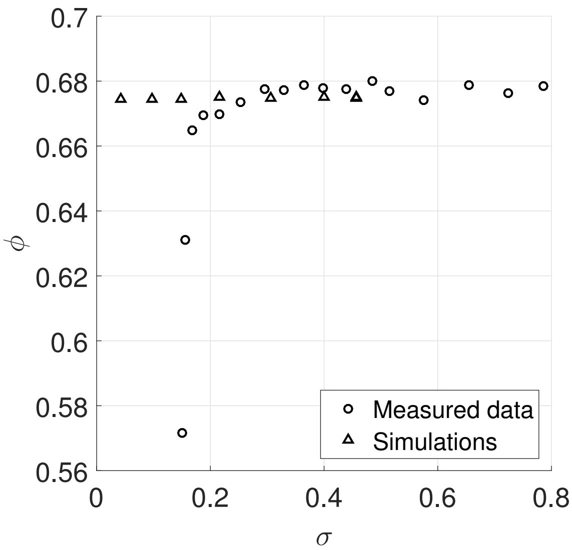

Figure 5.9: Comparison between measured data and simulations.

The cavitation is visualised by showing the areas where the surface pressure is below the vapour pressure. One example of this is shown in Figure 5.10, where areas below the vapour pressure is coloured in blue. This particular case have a flow rate coefficient ϕ=0.6639 and head rise coefficient ψ=2.825. These numbers are not exactly correspondent to a case presented by the John Hopkins University(ϕ=0.664, ψ=2.64) but are somewhat in the same range as Chen et al. (2016).

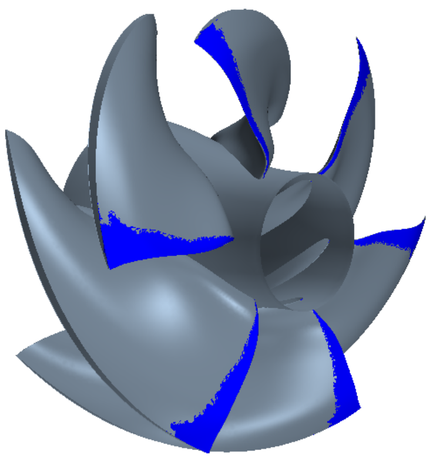

Figure 5.10: Pressure below the vapour pressure on the impeller surface

5.2 Wakejet pump performance

This section presents the results for the simplified waterjet unit are presented. In Figure 5.12 the pump efficiency and head rise are plotted as functions of the volumetric flow rate Q for the two rotational models MRF and RBM. The section starts with results to analyse the mesh quality and goes on to show pump performance curves, tip leakage, limiting streamlines, swirl vectors as well as results from the tip clearance study.

5.2.1 Mesh quality

In order to determine whether the chosen wall distance is appropriate, i.e. so that the first node is placed at $y^+ \simeq 1$ (see Section 3.4.1), the wall y^+ values are illustrated on the waterjet surfaces for the highest velocity simulated.

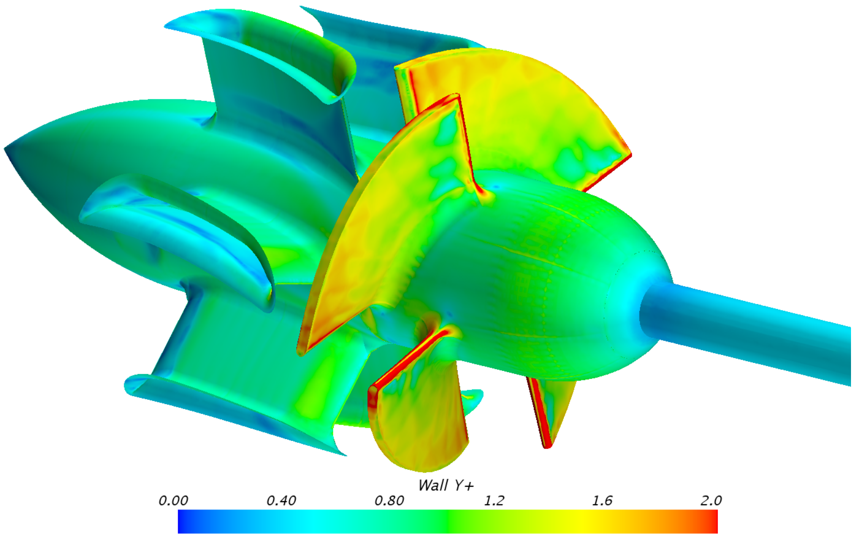

Figure 5.11: y^+ values for the first node on the simplified waterjet mesh at V_1=6 m/s with the impeller rotating at 6500 RPM using MRF.

Moreover, the volume change ratio between 1.0-0.1(Appendix A.5) is approximately 98.5% for all Wakejet waterjet models.

5.2.2 Pump performance curves

Figure 5.12 presents the calculated efficiency and head rise curves for the impeller with a tip clearance of 1 mm at 6500 RPM. Crosses represent results from RBM simulations whereas circles represent MRF simulations.

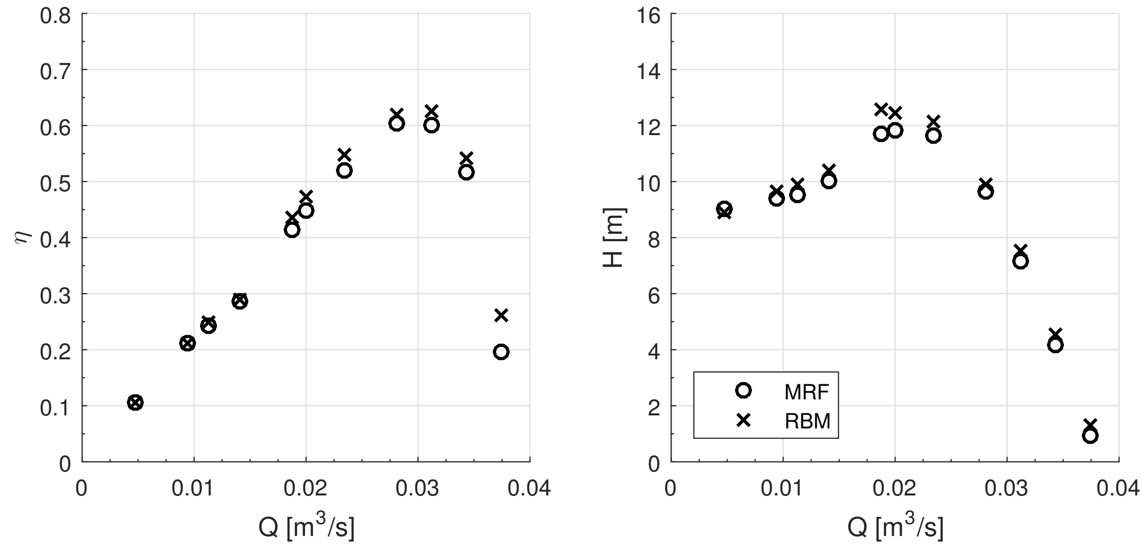

Figure 5.12: Comparison between MRF and RBM regarding efficiency and head rise over volumetric flow rate for the impeller with h=1 mm simulated at a fixed RPM of 6500.

The two simulation techniques follow each other fairly closely for all flow rates even though RBM simulations show slightly higher efficiency and head rise for most simulations. The maximum efficiency is found to be 62.5% at an inlet flow of 5 m/s using RBM. Since the two techniques show similar results no RBM simulations will be performed for any other tip clearance model.

Tip clearance study

Figure 5.13 shows the simulated effect of impeller tip clearance on the efficiency and head rise of the waterjet system. The impeller with h=1.0 mm is the impeller used in the Wakejet.

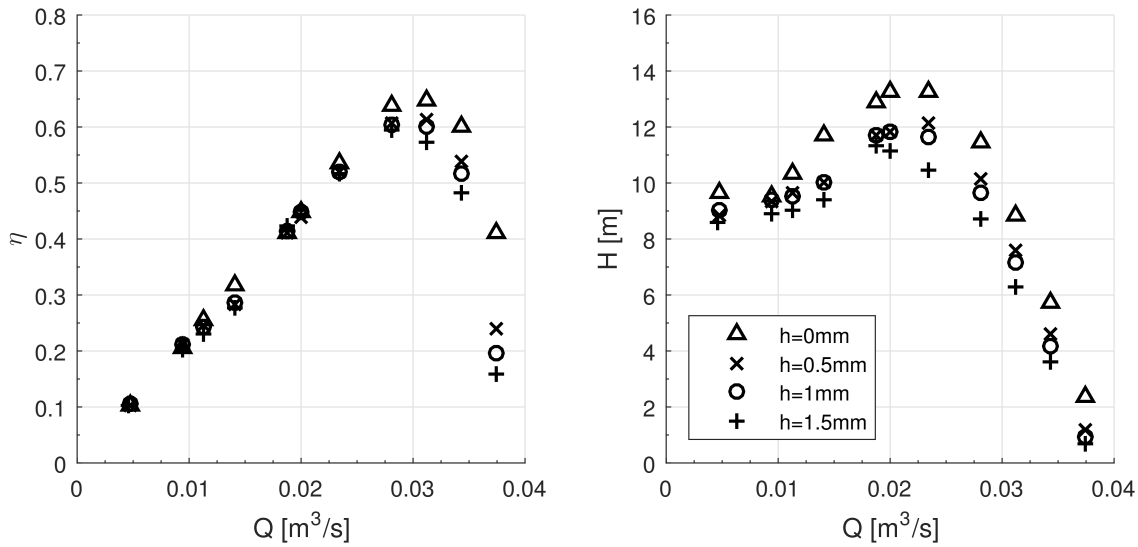

Figure 5.13: Efficiency and head rise over volume flux for all four impellers simulated at a fixed RPM of 6500 using MRF.

Tables showing exact values for head rise and efficiency over volume flux for all impellers can be found in Appendix A.4

5.2.3 Pump flow

Figure 5.14 shows an iso-surface of flow going in the reversed flow-direction on the impeller for three different inlet speeds. Tip leakage occurs when the iso-surface (blue) is located at an impeller blade tip. Moreover, Figure 5.15 shows a well developed TLV in the impeller tip region.

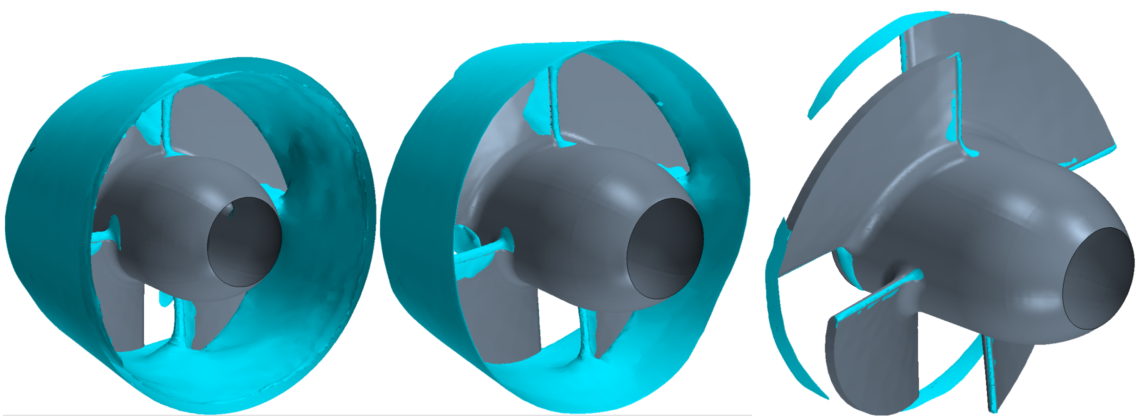

(a) V_1=0.75 m/s. **(b)** V_1=3.2 m/s. **(c)** V_1=6 m/s.

Figure 5.14: Illustration of water flowing in the opposite direction in the tip clearance region, for impeller with h=1 mm at 6500 RPM using MRF.

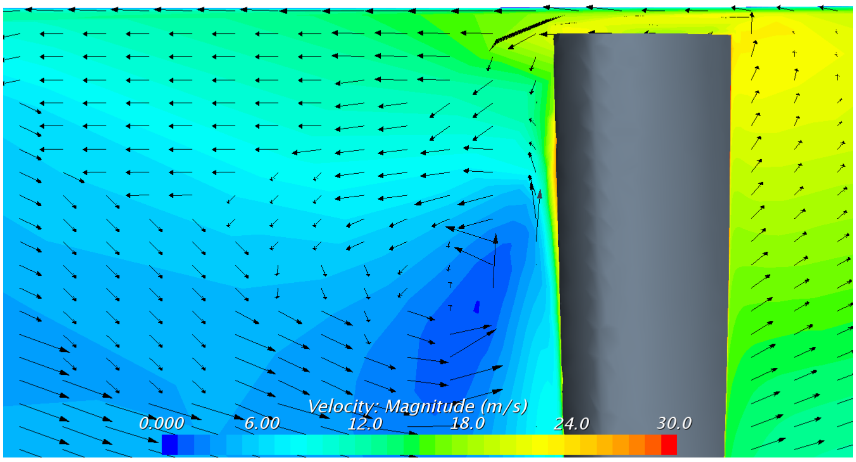

Figure 5.15: TLV at an impeller blade with h=1 mm running at 6500 RPM and board speed of 10 knots.

The limiting streamlines on impeller and stator are shown in Figure 5.16. It is clear from looking at the figure that there is a high risk of separation on the leading edge on the suction side of the impeller as well as the leading edge on the pressure side and trailing edge on the suction side of the stator blades. This should affect the performance of the pump negatively.

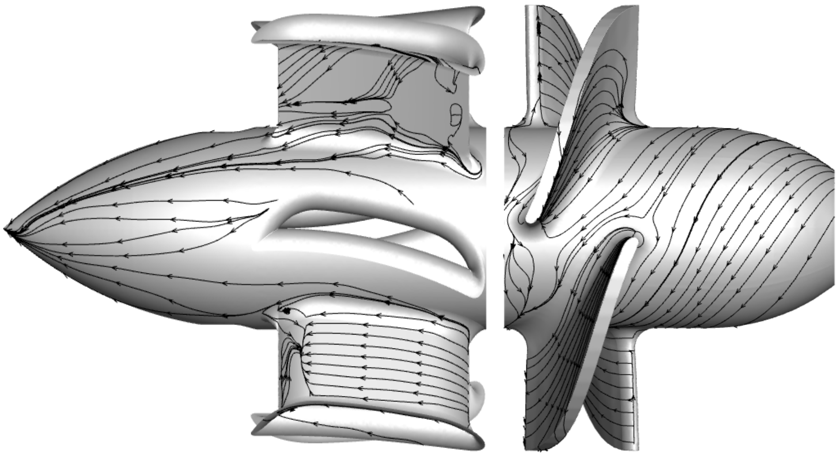

(a) Stator. **(b)** Impeller.

Figure 5.16: Limiting streamlines on the Wakejet waterjet system with an inlet speed of V_1=6m/s the impeller rotating at 6500 RPM using MRF.

The streamlines in the single fluid volume are shown in Figure 5.17.

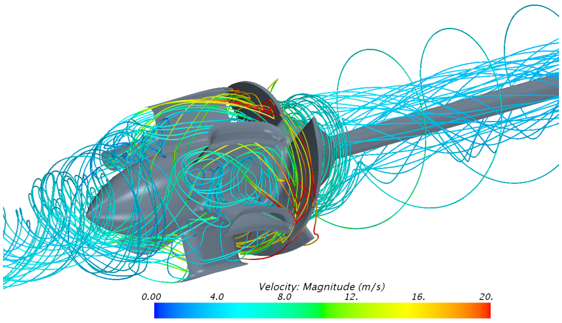

(a) V_1=0.75m/s.

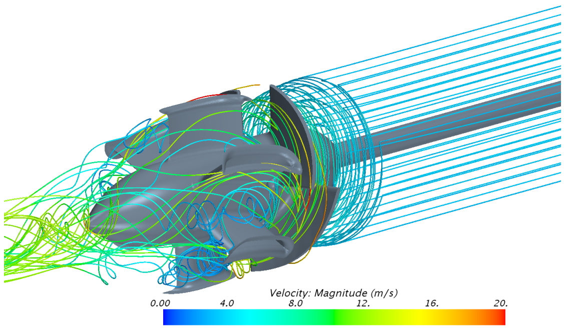

(b) V_1=3.2m/s.

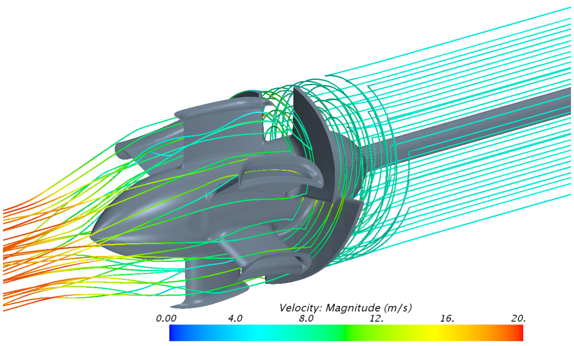

(c) V_1=6m/s.

Figure 5.17: Streamlines in the Wakejet waterjet system with for three different inlet speeds with the impeller rotating at 6500 RPM using MRF and a tip clearance of 1mm.

Swirl vectors at different positions in the waterjet system are shown in Figure 5.18.

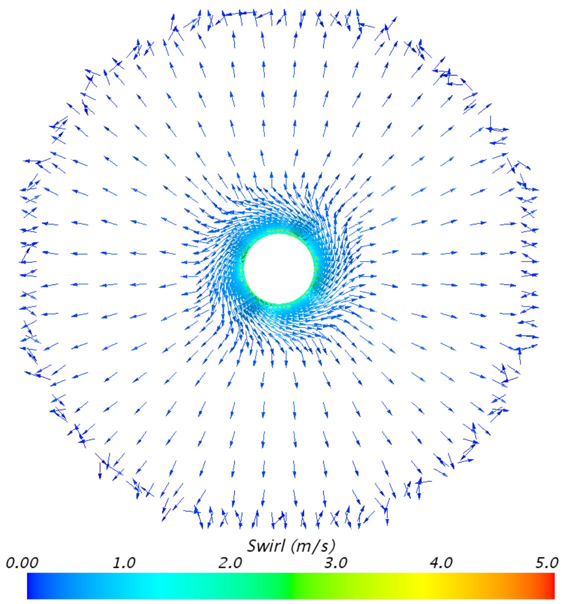

(a) Before impeller.

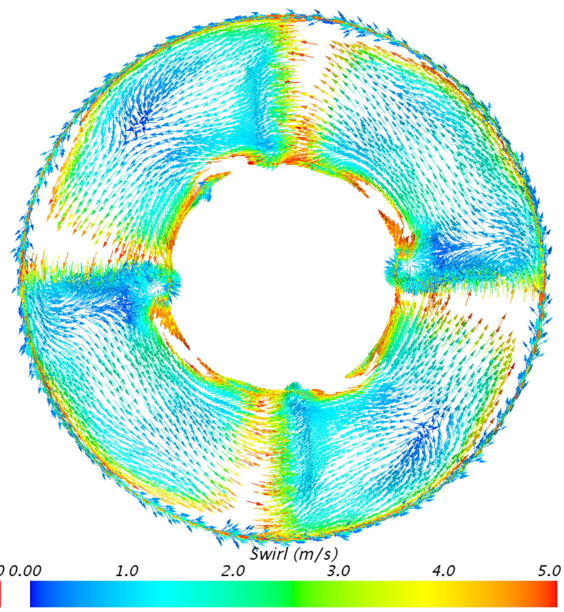

(b) Between stator and impeller.

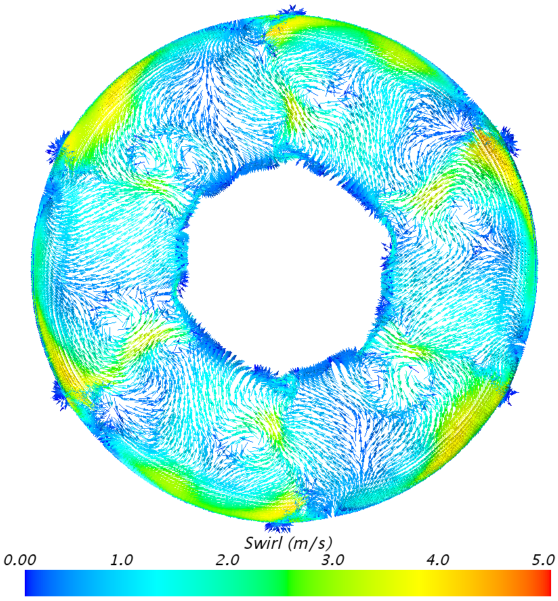

(c) After stator.

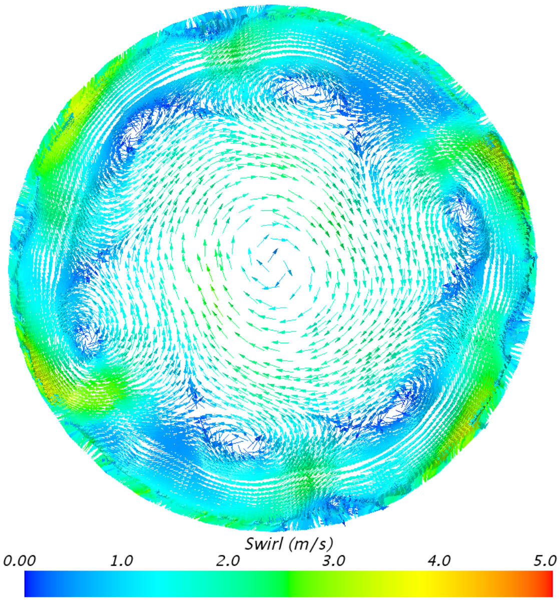

(d) At the outlet.

Figure 5.18: Swirl vectors at four different positions inside the Wakejet waterjet going at 6500 RPM using MRF at V_1=6m/s.

Both Figures 5.16 and 5.17 show that there is in fact a chaotic behaviour of the outlet flow. All velocities that are not in the axial direction can be seen as pure loss of kinetic energy as should in the ideal case be zero. Further on, in Figure 5.19 the impeller and stator torque is shown. Once again, it is shown that the stator does not counteract the swirl of the flow generated by the impeller except in the higher flow rate region (above Q=0.32 m^3/s). Another important observation to note in Figure 5.17a is the flow spiralling close to the wall upstream of the impeller. This flow moves in the reversed direction in comparison to the inlet flow direction. This indicates the existence of flow blockage at lower flow rates.

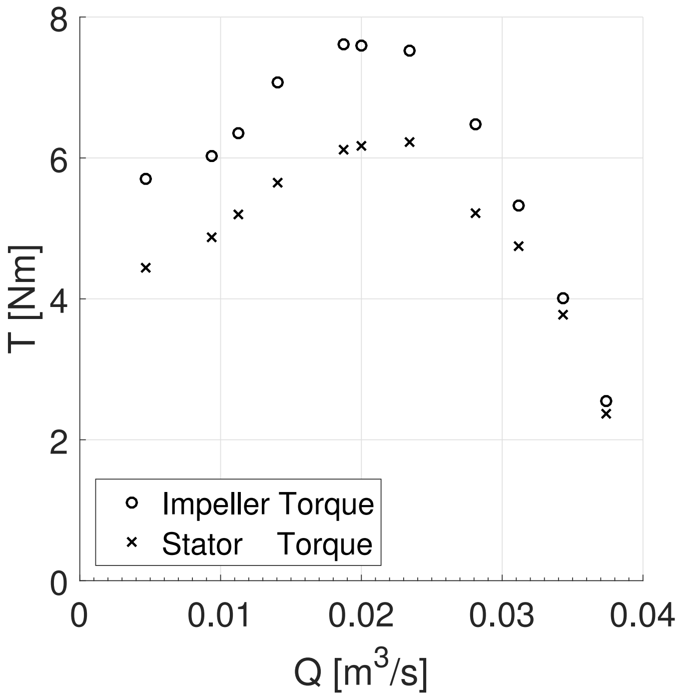

Figure 5.19: Comparison between impeller (h=1mm) and stator torque magnitude for the Wakejet waterjet simulated at a fixed RPM of 6500 using MRF.

5.2.4 Cavitation

When looking at the cavitation for the Wakejet pump there have been difficulties of matching the set-up used for the AxWJ-2 pump. The main area of uncertainty is regarding boundary conditions of the pressure since this is not stated in any report from John Hopkins University. Instead, the cavitation pattern is analysed on the whole Wakejet model where the pressure is atmospheric at the outlet, see section 5.3.4.

5.3 Wakejet performance

This section presents results from simulations performed on the whole Wakejet when it is fixed in all directions. The section starts with results to analyse the mesh quality and goes on to present results for the intake grill study, risk of cavitation and free surface.

5.3.1 Mesh quality

In order to determine whether the chosen wall distance is appropriate, i.e. so that the first node is placed at $y^+ \simeq 1$ (see Section 3.4.1), the wall y^+ values are illustrated on the waterjet surfaces for the highest velocity simulated.

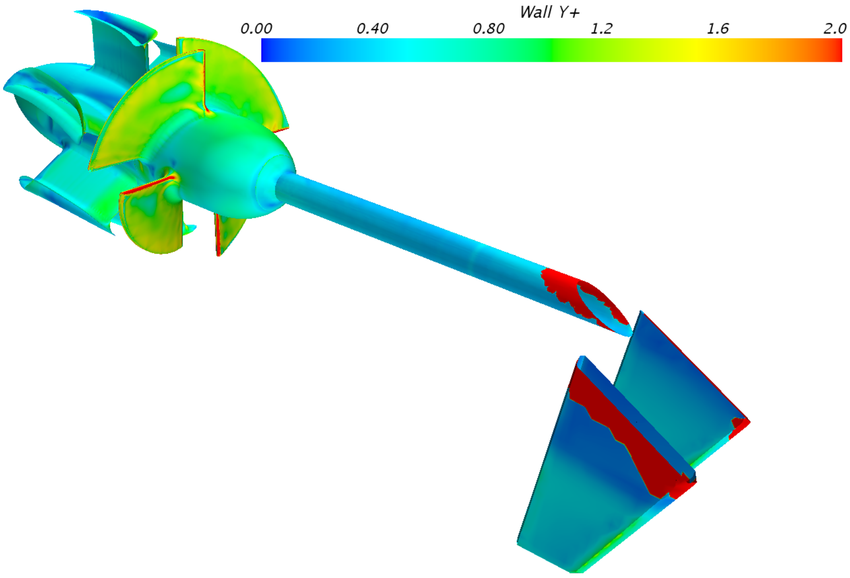

Figure 5.20: y^+ values for the first node on the Wakejet mesh at V_s=25 knots with the impeller rotating at 6500 RPM using MRF.

To analyse mesh quality the Courant number is visualised over the whole domain. As explained in Section 3.4.3 should be less than one.

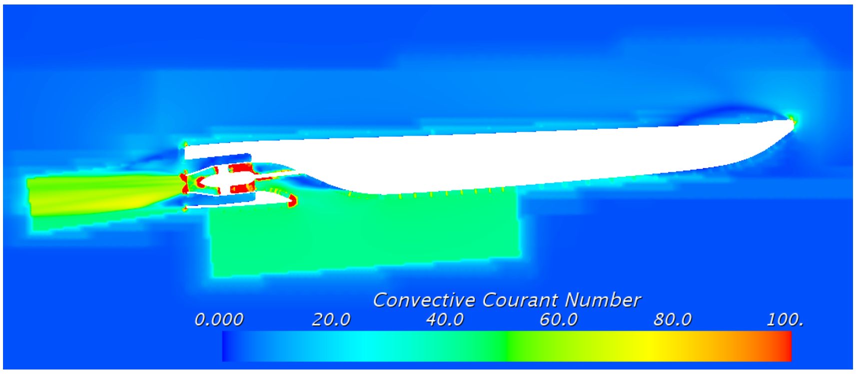

Figure 5.21: Courant number for the mesh on the Wakejet mesh at V_s=25 knots with the impeller rotating at 6500 RPM using MRF with a fixed trim of 2 degrees.

Moreover, the volume change ratio between 1.0-0.1(Appendix A.5) is approximately 98.4% for the Wakejet model.

5.3.2 Free surface

Figure 5.22 shows the volume fraction of water around the Wakejet. A numerical error is found close to the board surface and especially around the centre line of the Wakejet, where it seems that air is sucked into the waterjet system.

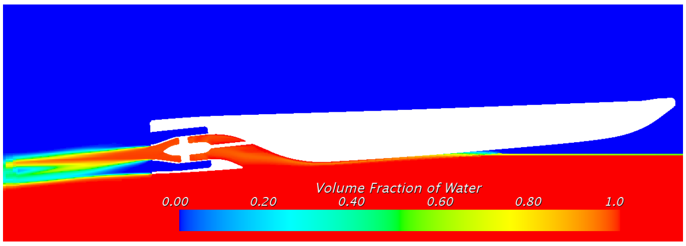

(a) Domain.

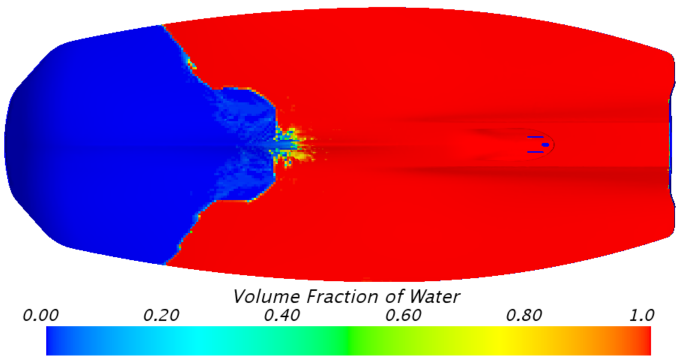

(b) Board seen from below.

Figure 5.22: Volume fraction of water in the system for the Wakejet going at 25 knots with the impeller rotating at 6500 RPM using MRF and a fixed trim of 2 degrees.

The Wakejet was successfully simulated in a totally fixed position relative to the water surface, Figure 5.23. This resulted in slight over prediction of both lift as well as a negative drag, indicating that the impeller should rotate faster than 6500 RPM in a self-propulsion test.

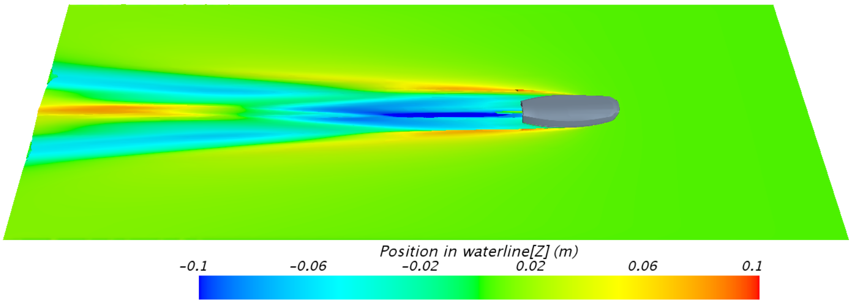

Figure 5.23: Free surface for the Wakejet going at 6500 RPM at 25 knots using MRF with a fixed trim of 2 degrees.

Free surfaces for other types of set-ups, such as free trim or fixed four degree trim, can be seen in Appendix A.6.

5.3.3 Intake grill study

Figure 5.24 shows vorticity together with velocity vectors in the intake of the Wakejet waterjet system with and without intake grills. The figure with intake grills clearly have a bigger separation region in the region near the roof. Figure 5.25 shows the inlet velocity profile for the two cases. The effect of the intake grills does seem to diminish when approaching the impeller.

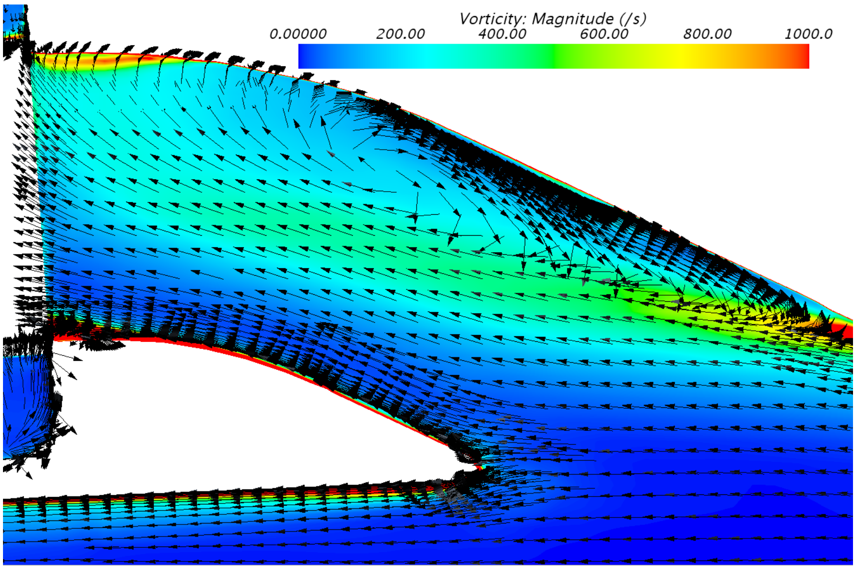

(a) Without intake grills.

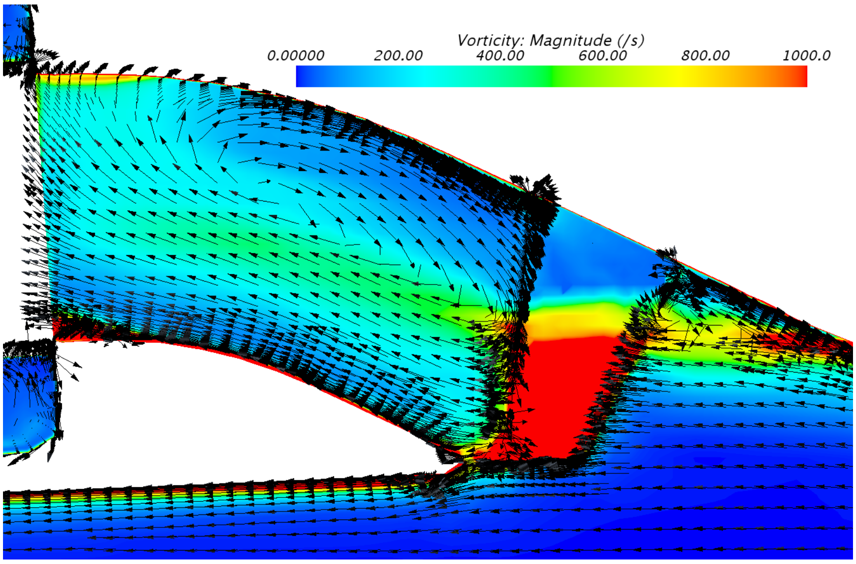

(b) With intake grills.

Figure 5.24: Vector field and vorticity magnitude in the waterjet system for the Wakejet going at 6500 RPM at 25 knots using MRF.

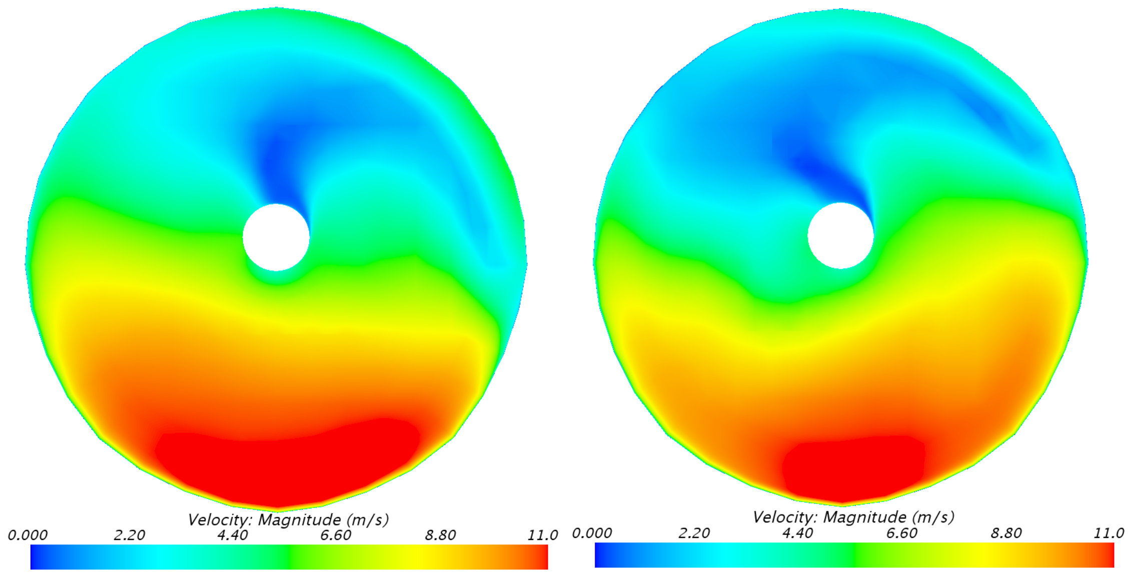

(a) Without intake grills. **(b)** With intake grills.

Figure 5.25: Velocity profile upstream of the impeller for the Wakejet going at 6500 RPM at 25 knots using MRF.

5.3.4 Cavitation

An iso-surface showing areas where the pressure drops below vapour pressure (3140 Pa) for water on the impeller and stator for the Wakejet going at 25 knots and the impeller rotating at 6500 RPM using MRF can be seen in Figure 5.26. The figure shows signs of hub vortex cavitation on the stator as well as sheet cavitation on the leading edge of the suction side of the impeller.

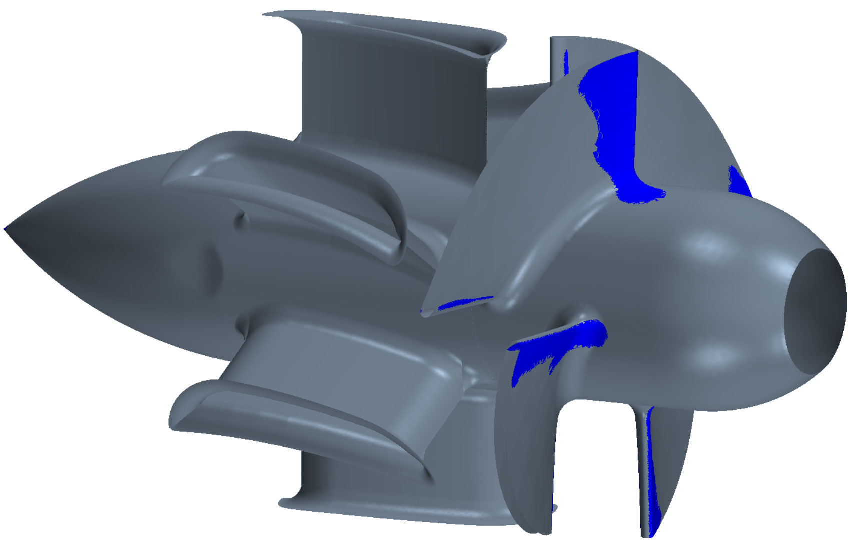

Figure 5.26: Iso-surface for vapour pressure of water on the stator and impeller for V_s=25 knots and the impeller rotating at 6500 RPM using MRF.

6 Discussion

This section provides a discussion regarding the results presented in Section 5. Mesh quality is discussed for all models. The two pumps, AxWJ-2 and Wakejet waterjet, are compared to each other when it comes to performance indicators such as efficiency, head rise, tip leakage and cavitation. Moreover, the AxWJ-2 simulation results are compared to measurements conducted at John Hopkins University. When it comes to the Wakejet model, grill intake effects and self-propulsion results are treated thoroughly.

6.1 Validation of AxWJ-2 performance

When it comes to analysing the validation study of AxWJ-2 pump performance it is important to make sure that the set-up used in STAR-CCM+ matches the set-up used at John Hopkins University as much as possible, which it in large parts does. It is however important to note that there are some key differences between the two set-ups. One difference is that the STAR-CCM+ model uses water as the liquid whereas a sodium iodide (NaI) is used at the test facility. The density, the viscosity and the vapour pressure are matched to the liquid NaI solution. The density and viscosity of the gas phase of the liquid are however unchanged due to difficulties finding reliable data. The pump performance is dominated by the difference in pressure between point 1 and 2 ($p_1 - p_2 = \Delta p$), the efficiency and head rise curves will not be affected by this change in fluid as the dynamic pressure difference is unaffected by the liquid and the static pressure difference is normalised with the density of the liquid. The NaI solution does have a higher viscosity which should lead to more frictional losses in the system. The head calculations, shows however little or no difference between the liquids used.

The cavitation simulations are on the other hand dependent on the inlet pressure and the vapour pressure as well as the the properties of the fluid in both liquid and gas phase. This could lead to some differences between the model and measurements as the exact conditions are hard to mimic. When comparing the flow coefficient to the cavitation number in Figure 5.9 it is clear that the simulations do not experience the same cavitation breakdown and heavy decrease in flow coefficient as the measurements. It has been noticed that the cavitation model is very sensitive to the boundary conditions that are applied and that matching the simulations to reality is very challenging. Imagery from the John Hopkins University shows that a change in just 2 kPa could change the cavitation pattern substantially.

Figure 5.10 provides however means to analyse risk of cavitation simply by looking at the parts on the surface where the pressure drops below vapour pressure, i.e. where cavitation should occur. When comparing with images from John Hopkins University it is clear that this way of analysing cavitation shows the correct type of cavitation but not the magnitude of it. The figure should thus only be seen as an indication of where cavitation could occur.

Another difference between the models is that the casing diameter is 304.26 mm in the CAD-model whereas it is 304.8 mm in the physical model. This difference affects the inlet velocity slightly since the flow rate is matched to the measurements. Notable is that the fit of the calculations to the data in Figure 5.3 is highly dependent on the input diameter. The inlet diameter in the model is 304.26 mm however if the expected flow rate is calculated backwards from the flow coefficient, the diameter should be 299.8 mm. This difference depends on the impeller shaft occupying some volume inside the the inlet channel and thus reducing the flow rate. Physically this has a little effect on pressure and velocities but some concern should be taken when calculating the flow- and head rise coefficients. The efficiency is however not effected by this and is still close to the measured values. The difference in casing diameter does affect the tip clearance and hence the tip leakage could differ between simulations and physical tests.

The last uncertainty regarding the set-up in STAR-CCM+ is regarding the location of diameter increase which should occur after the outlet. No exact position could be found in articles treating AxWJ-2 but had to be visually estimated in Figure 4.8, which could affect the outlet pressure if not placed incorrectly. All in all however, the results from STAR-CCM+ are shown to match the measured data in Figures 5.2 and 5.3 in a good manor. The maximum efficiency is calculated to be 89.55% which is very close to the 89% presented by Chen et al. (2016).

Regarding mesh quality the thickness of near wall prism layer seems to be fitting since the wall y^+ values are below one almost everywhere. The only area where the values are over one is near the leading edge on the suction side of the impeller blades but since the values still are close to one no problems regarding y^+ should arise. The volume change ratio is also in a good shape even though some refinements could be done in the tip clearance region to further raise the 1-0.1 ratio from 96.5%.

Flow features such as swirl, limiting streamlines and tip leakage are important in order to be able to make conclusions on the Wakejet waterjet. The limiting streamlines on the impeller and stator for the AxWJ-2 (Figure 5.5) show a smooth flow across the blades with few signs of separation. As seen in Figure 5.4, there is some tip leakage. However, the amount of leakage is not large and should not affect the performance significantly. Lastly, the shown swirl vectors over the waterjet system in Figure 5.7 show that all parts of the system work together in a good manor since the outlet swirl is of a low magnitude with only small vortices close to the wall. Figure 5.6 further shows how the well designed stator show little signs of separation and Figure 5.8 shows a ratio between impeller and stator torque close to one.

6.2 Wakejet pump study

Something to keep in mind when it comes to analysing the performance of the Wakejet waterjet pump is the alterations made to the impeller and stator. In the provided CAD geometries the blades on impeller and stator were cut off and did not have a smooth transition on neither leading or trailing edges of the stator and the trailing edges of the impeller blades. That design would lead to a high risk of separation of flow on the trailing edges of impeller and stator as well as blockage of flow on the leading edge of the stator, making the provided design far from ideal. This would also mean that the mesh would have to be very fine in these areas to capture the rapid flow changes, increasing the number of cells used even further. If the pump used on the Wakejet does have these cut offs of the blades it is highly recommended that they are re-designed as in Figure 4.3.

The y^+ values shown in Figure 5.11 show higher values compared to the y^+ values on the AxWJ-2, but the values are still approximately equal to one. The only exception is on edges of the impeller blades where the values maximum value is as high as 3.8, which is not optimal. The problem was however not considered significant enough to refine the mesh further on the impeller blade edges. When it comes to mesh quality, the values of the face validity are as high as around 98.5% for the 1.0-0.1 range. The mesh is over all well functioning and does not need any alterations, except possibly on the impeller blades.

The set-up used for the Wakejet waterjet performance simulations is made to match the one used on the AxWJ-2 by scaling all parameters using the diameter of the casing. The only uncertainty is, again, regarding the location of the increase of diameter after the outlet. The chosen location is however placed at exactly the same location as in the AxWJ-2 scaled by diameter. The two set-ups should thereby match each other and the generated performance curves thus be viable.

When it comes to analysis of the performance curves it quickly becomes clear that the design of the pump is far from optimal. The maximum efficiency is found the be around 62% which in itself is fine, the main problem is the steep rise and fall of the efficiency curve. As shown in Figure 5.12, the maximum efficiency point occurs for an inlet speed of 5 m/s, which corresponds to a board speed between 15 and 20 knots. For a product such as the Wakejet however it is the maximum speed (25 knots) that is the most relevant to look at, especially considering that Radinn has declared an interest in increasing the maximum speed to 30 knots. It should be noted that the inlet speed is an approximation taken from simulations of the Wakejet and could differ from reality. The efficiency at 25 knots is as low as 26% (RBM) showing a rapidly decreasing efficiency at higher speeds. The efficiency is low at the slower speeds as well but these speeds are not as significant since the typical rider rapidly accelerates the Wakejet to the fastest speed possible. Moreover, it is also probable that the impeller shaft rotates slower than 6500 RPM on lower speeds, which affects the efficiency. Performance curves should therefore be performed on several additional RPM based on data collected from physical tests in order to further evaluate the performance of the Wakejet. The MRF vs. RBM study conducted shows that the MRF technique is good enough to simulate rotation of the impeller except maybe for the highest speed, where the difference between the two efficiency curves is 30%.

The tip clearance study shows that the efficiency could be increased quite significantly simply by reducing the tip clearance from 1mm. According to the performed simulations, the optimal tip clearance would be at 0mm giving an efficiency of 41% (MRF) at the highest speed, keeping in mind that RBM probably would show even higher values. STAR-CCM+ does not take frictional losses into account, which would be significant for a tip clearance equal to zero, i.e. having the impeller blade tip rotating on the casing, which makes the 0mm case an unrealistic choice. What the simulations show however is that having an as small tip clearance as possible is desirable for this waterjet. This also becomes a question of production technique, where a lower tip clearance requires a more precise production technique.

Another problem related to the tip clearance is tip leakage. As shown in Figure 5.14, the amount of reversed flow in the tip region is quite severe, especially at lower speeds. Figure 5.17 shows how the large amount of tip leakage causes a blockage of flow in the tip region for the lowest speed, causing the streamlines to be drawn towards to shaft before reaching the impeller as well as reverse flow near the wall downstream of the impeller. Additionally, Figure 5.14 shows a well developed TLV for an inlet speed of 3.2 m/s, further illustrating the problem in the tip region. Once again, a reduced tip clearance could improve the overall performance of the pump. It is however difficult to quantify the effect of tip leakage on the performance, but it is fair to assume that a smaller amount of tip leakage is favourable.

By looking at the limiting streamlines on the stator and impeller in Figure 5.16 it is possible to draw further conclusions regarding the design of the pump. It seems like the impeller is fairly well-designed with few signs of separation, except for at the leading edge on the suction side where the streamlines are drawn away from the edge. For the stator however the story is very different. Even though the suction side seems to be working fine except towards the trailing edge, the pressure side does experience separation on large parts of the surface. The streamlines show separation both on the leading and towards the trailing edge, probably affecting the performance in a negative way since the outlet is located directly aft of the stator cone. Figure 5.17 further helps illustrate the problem with the stator, where the flow behaves chaotically in between the stator blades. Figure 5.18 shows the swirl vectors at four different positions in the waterjet system. The figure illustrates the problem with the stator, since both Figures 5.18c and 5.18d have quite significant vortices with high magnitudes close to the wall. Figure 5.19 also shows the problem with regards to the stator since it does not produce enough torque to counteract the impeller, especially on low and medium flow rates.

When comparing the impeller hub of this pump to the hub of other pumps it seems as it has a rather blunt shape. The time limit of this project has made it hard to examine the effect of this, but having a smoother transition between impeller shaft and hub could help improving the inflow to the impeller.

6.3 Wakejet study

The y^+ values for the Wakejet model show similar results as the Wakejet pump only with the addition of having very high values (up to 310) close to the wall for the impeller shaft and intake grills. This indicates that the near wall distance should be decreased significantly. Moreover, by looking at the Courant number (Figure 5.21) it becomes clear that convergence problems could arise due to the high Courant numbers inside the waterjet unit when using RBM. The problem with Courant number can be fixed either by decreasing the time-step or making the mesh more coarse. Making the cells larger inside the waterjet is however not recommended since this could cause the geometry to be represented in a bad manor.

Additionally to the non-optimal mesh quality, a numerical error regarding the volume fraction of water in the waterjet system has been discovered, as was feared in Section 4.2.8. It seems like air is sucked under the board and inside the waterjet system, something that is not very physical. This could possibly lead to the resistance of the board being under-predicted and also to wrongly distributed hydrodynamic lift forces since the board is going partly in air. In Figure 5.22 a source term drawing air away from the waterjet has been added to the model. The term has shown improved results regarding the air in the system, although some air still does occur in in the channel. More work could then be done in order to solve the problem entirely, keeping in mind that the source term may cause nonphysical effects such as water rising higher on the board.

One problem that has arisen in this project is the convergence rate of the Wakejet model. The goal has always been to perform full self-propulsion simulations in order to analyse flow in the waterjet and around the hull in conditions that will match reality as much as possible. Partly due to the poor mesh quality, as described above, only a few simulations with free sinkage and a rotating impeller has been able to converge. Several different ways of solving the problem have been tested, for example a simulation was run using the "Convective CFL Time step control" model activated. This model adjusts the time-step of the simulation according to a targeted Courant number. Unfortunately this resulted in the model always choosing the shortest time-step possible (10^{-6}s) which lead to an unreasonable amount of computational time in order to achieve any results. Several attempts on refining the mesh inside the waterjet has also been performed with no improvements on the convergence. Moreover, it seems like the length of the domain could be made even longer since the large wave pattern from the Wakejet sometimes causes reversed flow on the outlet boundary, which also affects the convergence rate negatively.

The choice of trim is also something that heavily affects the convergence rate. Simulations with no trim and free sinkage have been able to converge with the drawback of the Wakejet not being able to produce enough lift and thus ending up below the free surface as can be seen in Figure A.2 in the Appendix. The Wakejet model was however successfully simulated in a totally fixed position, with the impeller rotating at 6500 RPM, as shown in Figure 5.23 (Appendix A.6). Unfortunately, this way of performing self-propulsion tests leads to a great increase in the number of simulations since one simulation only handles one sinkage and one trim angle. Full self-propulsion tests have thus not been done due to the lack of time, but only on 25 knots and at 6500 RPM with a 75kg rider. What would have been interesting to examine is the optimal trim and waterline levels for different rider weights as well as required impeller rotational speed.

What can be said using these simulations is the inlet speed to the impeller, as described in Section 4.4.1, as well as flow effect due to the intake grills. One concern in the beginning of the project was that the intake grills would create separation and large vortices due to their blunt shape. Since the pump efficiency is not calculated on the Wakejet model it is difficult to quantify the exact effect on the performance, but the effect can be analysed visually. As seen in Figures 5.24 and 5.25 it seems that the grills in fact do not affect the inlet flow significantly. Even though the separation region near the intake roof is bigger when having the grills the effect of them seem to diminish when approaching the impeller which explains the small difference between the results of the inlet velocity profiles. Both inlet velocity profiles in Figure 5.25 show however a far from uniform inflow to the impeller. The difference in velocity can be derived from the shape of the intake which will accelerate the flow close to its curvature. Figure 5.24 also shows that separation occurs at the roof of the intake contributing further to the non-uniform velocity profile. In order to achieve a more uniform inflow to the impeller, as is desirable, a re-design of the intake could thus be necessary. It is also possible that a different design of the intake grills in fact could help decrease the separation region, so a study could also be done on the shape of the intake grills.

Moreover, Figure 5.26 shows that the Wakejet impeller could experience cavitation on both the impeller and stator hubs as well as sheet cavitation on the leading edges of the impeller. The boundary conditions are in this case is known, as the Wakejet operates under atmospheric pressure. The pressure distribution should thus be correct in this sense but could differ due to different trim and the numerical error described previously. Cavitation could cause a number of different effects but the main focus in this project has been on the possible effects on performance since wear should not be a problem because of the few operational hours of a Wakejet.

7 Conclusions

As discussed in Section 6, the performance of the AxWJ-2 axial pump has been calculated and validated by comparing set-up and data from physical experiments. The calculated performance is matched to data in a good manor. However, cavitation results can not be validated as the simulations does not match reality sufficiently. The cavitation results could however be used as an indication of where cavitation could arise.

The pump has a maximum efficiency of approximately 63% at a Wakejet speed of approximately 15 knots, but the efficiency goes as low as to 20% for the highest Wakejet speed of 25 knots. However the inlet velocity of the Wakejet is not validated so the efficiency at a certain speed may not correspond to reality, but the overall appearance of the the Wakejet waterjet performance curves should be considered valid since the simulations have used the same set-up as for the AxWJ-2 pump. Moreover, it is shown that great amounts of separation occurs inside the waterjet system of the Wakejet. Especially the stator would need a re-design in order to better direct the flow towards the outlet. Results also indicate that the tip clearance of the impeller should be made as small as possible.

Unfortunately, self-propulsion simulations have not been fully performed. The main problem with the convergence rate can be derived from the high y^+ number that is found inside the waterjet system and reversed flow on the outlet boundary. In order to perform self-propulsion tests in the future focus should be on decreasing the Courant number either by decreasing time-step or increasing cell-size. Alternatively a body force model (momentum source) can be used to model the pump. The performed Wakejet simulations shows however that the intake grills do not affect the inflow significantly despite their blunt appearance. Moreover, the inflow to the impeller is found to be non-uniform which should affect the performance negatively. A redesign of the intake shape could improve the inflow.

A list of possible ways of increasing the overall performance of the Wakejet can be found below.

- Re-design blades on impeller and stator, as supposed to the original design with cut-off blades (Section 4.1.1)
- Redesign of stator blades in order to avoid separation on pressure side and reduce outlet swirl (Section 5.2.3)
- Decrease tip clearance to as small as possible (Section 5.2.2)
- Redesign of intake to make inlet velocity profile more uniform (Section 5.3.3)

8 Future work

Due to the time limit that comes with the project together with the convergence issues on the Wakejet that are discussed in Section 6.3, a few important results are missing. In order to further evaluate the Wakejet performance a list of recommendations for future work can be found below.

- Wakejet waterjet studies on several RPM
- Studies on additional tip clearances in range between 1 and 0 mm
- Reduce near wall distance for mesh on impeller shaft and intake grill to prevent high y^+ and Courant number values
- Find optimal trim different Wakejet speeds and rider weights
- Move domain outlet downstream in order to avoid reversed flow on the outlet boundary
- Thorough investigations of the Wakejet's cavitation behaviour and its effect on the performance
- Further improve source term that affects the thin air layer underneath the hull and analysis of possible nonphysical effects (Sections 4.2.8 and 5.3.2)
- Investigation of a smoother transition between impeller shaft and impeller hub
- Look into the intake grills' effect on resistance and investigate other designs to reduce separation region
- Investigate possibility of optimisation of Wakejet hull shape with regards to resistance

References

Andersen, Johan and Gustav Moe (2014). *Systematic variations of parameters affecting waterjet-hull interaction, M.Sc. Thesis*. Gothenburg, Sweden: Department of Shipping and Marine Technology, Chalmers University of Technology.

Borret, Dick and Philip Rae (2008). “Waterjet Applications in Vessels that Operate in Multiple Modes”. In: *Waterjet Propulsion 5*. London, UK: The Royal Institution of Naval Architects. Chap. 1.

Brizzolara, Stefano and Diego Villa (2010). “CFD SIMULATION OF PLANING HULLS”. In: Seventh International Conference on High-Performance Marine Vehicles. Melbourne, Florida, USA.

Bulten, Norbert W. H. (2006). “Waterjet propulsion theory”. In: *Numerical Analysis of a Waterjet Propulsion System*. Eindhoven, The Netherlands: Printservice Technische Universiteit Eindhoven. Chap. 2.

Bulten, Norbert W. H. and Bart P.M. van Esch (2007). *Fully Transient CFD analyses of waterjet pumps*. Tech. rep. Netherlands and Eindhoven, Netherlands: Wärtsilä Propulsion and Technische Universiteit.

Carlton, John (2012). “Waterjet Propulsion”. In: *Marine Propellers and Propulsion*. 3rd edition. Oxford, UK: Butterworth-Heinemann. Chap. 16.

Chen, Huang et al. (2016). *Effects of Circumferential Grooves on the Cavitation and Performance of an Axial Waterjet Pump*. Tech. rep. Baltimore MD, USA: (Department of Mechanical Engineering, Johns Hopkins University.

Davidsson, Lars (1997). *An introduction to turbulence models*. Gothenburg, Sweden: Department of Thermo and Fluid Dynamics, Chalmers University of Technology.

Dyne, Gilbert and Göran Bark (2005). “PROPELLER FUNDAMENTALS”. In: *SHIP PROPULSION, Compendium for part of the M.Sc. course "Ship resistance and propulsion"*. Gothenburg, Sweden: Shipping and Marine Technology: Division of hydromechanics, Chalmers University of Technology. Chap. 1.

Engineers Edge, LLC (2017). *Mass Moment of Inertia Equations*. URL: `http://www.engineersedge.com/mechanics_machines/mass_moment_of_inertia_equations_13091.htm` (visited on 03/17/2017).

Eslamdoost, Arash (2014). *The Hydrodynamics of Waterjet/Hull Interaction, Ph.D. Thesis*. Gothenburg, Sweden: Department of Shipping and Marine Technology, Chalmers University of Technology.

Faltinsen, Odd M. (2005). *Hydrodynamics of High Speed Marine Vehicles*. USA: Cambridge University Press.

Feldbrugge, Berend (2015). *Description of swirling outlet flow in a waterjet pump using STAR CCM+*. Internship. Gothenburg, Sweden: Department of Shipping and Marine Technology, Chalmers University of Technology.

Ferziger, Joel H. and Milovan Peric (2002). *Computational Methodes for Fluid Dynamics*. 3rd edition. Berlin, Germany: Springer-Verlag.

Fluent Inc. (2006). *Shear-Stress Transport (SST) k- ω Model*. URL: `https://www.sharcnet.ca/Software/Fluent6/html/ug/node487.htm` (visited on 05/09/2017).

Griffith-Jones, Gavin J. (1994). *Investigation of Incompressible Flow Through an Intake Duct with Applications to Waterjet Propulsion, Ph.D. Thesis*. Christchurch, New Zealand: Department of Mechanical Engineering, University of Canterbury.

ITTC (2011). "Recommended procedures and guidelines - Practical guidelines for ship CFD applications". In: 26^{st} International Towing Tank Conference, The Specialist Committee on CFD in Marine Hydrodynamics. Rio de Janeiro, Brazil.

Kang, Can et al. (2014). *Influence of stator vane number on performance of the axial-flow pump*. Tech. rep. Zhenjiang, China and Shanghai, China: School of Energy et al.

Krause, Egon (2005). *Fluid mechanics: with problems and solutions, and an aerodynamic laboratory*. Berlin Heidelberg: Springer.

Menter, Florian R. (1993). "Zonal Two Equation k-w Turbulence Models for Aerodynamic Flows". In: *AIAA* (93-2906). 24^th Fluid Dynamics Conference, July 1993.

Michael, Thad J. et al. (2008). *Design of the ONR AxWJ-2 Axial Flow Water Jet Pump*. Tech. rep. West Bethesda, USA: Naval Surface Warfare Center.

Miorini, Rinaldo L. et al. (2012). "The Internal Structure of the Tip Leakage Vortex Within the Rotor of an Axial Waterjet Pump". In: *Journal of Turbomachinery* Vol. 134 (032018-1).

Moon-Chan, Kim and Chun Ho-Hwan (2005). *Experimental Investigation into the performance of the Axial-Flow-Type Waterjet according to the Variation of Impeller Tip Clearance*. Tech. rep. Pusan, Korea: Department of Naval Architecture and Ocean engineering.

Onera (2011). *Separation in three-dimensional steady flows*. URL: `http://www.onera.fr/sites/default/files/ressources_documentaires/cours-exposes-conf/onera-3d-separation-jean-delery-2011-1b.pdf` (visited on 05/18/2017).

Peri, Daniele et al. (2012). "Simulation Based Design with Variable Physics Modelling and Experimental Verification of a waterjet propelled Catamaran". In: 29^{th} Symposium on Naval Hydrodynamics. Gothenburg, Sweden.

Radinn AB (2016). *Technical Specifications*. URL: `http://www.radinn.com/technology` (visited on 02/07/2017).

Radinn AB (2017). *Mail correspondence with Alexander Lind.*

Siemens PLM Software (2017). *STAR-CCM+ User Guide.* Christchurch, New Zealand: Siemens Product Lifecycle Management Software Inc.

Tan, David et al. (2015). "Experimental Investigation of the Role of Large Scale Cavitating Vortical Structures in Performance Breakdown of an Axial Waterjet Pump". In: *Journal of Fluids Engineering* Vol. 137 (111301-1).

van Terwisga, Tom J.C. (1996). *Waterjet-Hull Interaction.* Wageningen, Netherlands: Grafisch Bedrijf Ponsen & Looijen BV.

White, Frank M. (2011). *Fluid Mechanics.* 7th edition. USA: McGraw Hill.

Wu, Huixuan et al. (2012). "Tubulence Within the Tip-Leakage Vortex of an Axial Waterjet Pump". In: *AIAA Journal* Vol. 50, No. 11 (DOI: 10.2514/1.J051491).

Yamamoto, Kazuyoshi and Yoshinobu Tsujimoto (2009). *Backflow Vortex Cavitation and Its Effects on Cavitation Instabilities.* Tech. rep. Nomi Ishikawa, Japan and Osaka, Japan: Center for Research, Investigation of Advanced Science, and Technology, Engineering Science.

Yates, Leslie A. and Richard L. Fearn (1988). "The Determination of the Topological Structure of Skin Friction Lines on a Rectangular Wing-Body Combination". In: *NASA Contractor Report 4168.* Gainesville, Florida, USA: National Aeronautics and Space Administration.

A Appendix

A.1 Mesh values

Table A.1: Mesh values for the computational domain and board region.

Base size	100 mm
Maximum cell size	100% of Base size
Number of prism layers	25
Prism layer thickness	14.5 mm (Eq 3.14)
Thickness of Near Wall Prism layer	0.00252 mm (Eq 3.17)

Refinement on board faces	
Target size	18% of Base size
Minimum size	12% of Base size

Refinement on impeller, shaft and grill faces	
Target size	1% of Base size
Minimum size	1% of Base size
Prism layer thickness	5 mm

Refinement on feature curves	
Target size	10% of Base size
Minimum size	5% of Base size

Table A.2: Mesh values for the Impeller and Outlet and stator regions.

Base size	5 mm
Number of prism layers	25
Prism layer thickness	5 mm
Thickness of Near Wall Prism layer	0.00252 mm (Eq 3.17)

Refinement on feature curves	
Target size	0.25 mm
Minimum size	0.25 mm

Table A.3: Mesh values for mesh refining geometrical shapes.

Rectangular refinement of waterline	
Isotropic size	50% of Base size
Anisotropic Z size	8% of Base size

Triangular refinement of wake	
Isotropic size	25% of Base size
Anisotropic Z size	8% of Base size

Cylindrical refinement of jet stream	
Isotropic size	5% of Base size

Cubic refinement of area around hull	
Isotropic size	50% of Base size

Cubic refinement of area close to hull	
Isotropic size	25% of Base size

Cubic refinement of intake area to waterjet	
Isotropic size	5% of Base size

A.2 Physical conditions

Table A.4: Computational models used for the Wakejet simulations with free surface.

- Three Dimensional
- Implicit Unsteady
- Eularian Multiphase
- Volume of Fluid (VOF)
- Turbulent
- $k-\omega$ Turbulence
- Gravity
- VOF Waves
- All y^+ Wall Treatment
- Exact Wall Distance
- SST (Menter) $k-\omega$ (*For further details see Section 3.4.2*)
- Reynolds-Averaged Navier-Stokes
- Gradients
- Segregated Flow
- Multiphase Equation of State
- Multiphase Interaction

Table A.5: Parameters in 6DOF Body with the case of rider weighing 75kg.

Body	
Body Mass, m_{tot}	128.5 kg
Release time	2 s
Ramp time	20 s
Free Motion	
z motion	Enabled
Initial Values	
Centre of mass	[0.92, 0, 0.45] m
Moment of inertia, (Eq. 3.1)	[7.2, 39.0, 45.5] kg m^2

A.3 Solver properties and stopping criteria

Table A.6: Solver properties.

Implicit Unsteady	
Temporal Discretization	2^{nd} order
Partitioning	
Solver frozen	Enabled
Time-Step, MRF	0.025s
Time-Step, RBM	25.6*10^{-6} s (1°/time-step) *See Section 4.2.5*
Wall Distance	
Solver frozen	Enabled

Table A.7: Stopping Criteria.

Maximum inner iterations	
Enabled	
Maximum inner iterations	5
Maximum physical Time	
MRF simulations	20 s
RBM simulations	Disabled *See Section 4.2.5*
Maximum steps	
MRF simulations	Disabled
RBM simulations	720 additional time-steps *See Section 4.2.5*

A.4 Effect of impeller tip clearance

Table A.8: Efficiency for four different tip clearances using MRF and one using RBM at 6500 RPM.

	Q $[10^{-3}m^3/s]$										
h	4.7	9.4	11.2	14.0	18.7	20	23.4	28.1	31.2	34.3	37.4
0.0mm, MRF	10%	21%	26%	32%	41%	45%	53%	64%	65%	60%	41%
0.5mm, MRF	10%	21%	25%	28%	41%	44%	52%	61%	61%	54%	24%
1.0mm, MRF	11%	21%	24%	29%	41%	45%	52%	60%	60%	52%	20%
1.0mm, RBM	11%	21%	25%	29%	44%	47%	55%	62%	63%	54%	26%
1.5mm, MRF	10%	20%	23%	28%	42%	45%	52%	59%	57%	48%	16%

Table A.9: Head rise (m) for four different tip clearances using MRF and one using RBM at 6500 RPM.

	Q $[10^{-3}m^3/s]$										
h	4.7	9.4	11.2	14.0	18.7	20	23.4	28.1	31.2	34.3	37.4
0.0mm, MRF	9.7	9.5	10.4	11.7	12.9	13.3	13.2	11.5	8.8	5.7	2.4
0.5mm, MRF	8.9	9.7	5.5	10.0	11.7	11.8	12.1	10.1	7.6	4.6	1.2
1.0mm, MRF	9.0	9.4	9.5	10.0	11.7	11.8	11.6	9.7	7.1	4.2	0.9
1.0mm, RBM	8.9	9.6	9.8	10.4	12.5	12.4	12.1	9.9	7.5	4.5	1.3
1.5mm, MRF	8.6	8.9	9.0	9.4	11.3	11.1	10.5	8.7	6.3	3.6	0.7

A.5 Mesh size and quality

Table A.10: Mesh size and quality with respect to volume change for the six different models.

	No. of cells	**Volume Change Ratio**		
Overall Statistics		[1.0-0.1]	[0.1-0.01]	[0.01-0.001]
Wakejet	20 469 970	98.429%	1.545%	0.026%
Wakejet waterjet, $h = 0.0mm$	6 105 332	98.640%	1.351%	0.008%
Wakejet waterjet, $h = 0.5mm$	5 943 482	98.504%	1.459%	0.036%
Wakejet waterjet, $h = 1.0mm$	5 988 658	98.505%	1.468%	0.026%
Wakejet waterjet, $h = 1.5mm$	6 011 260	98.711%	1.265%	0.024%
AxWJ-2	6 653 940	96.510%	3.291%	0.192%

A.6 Free surface

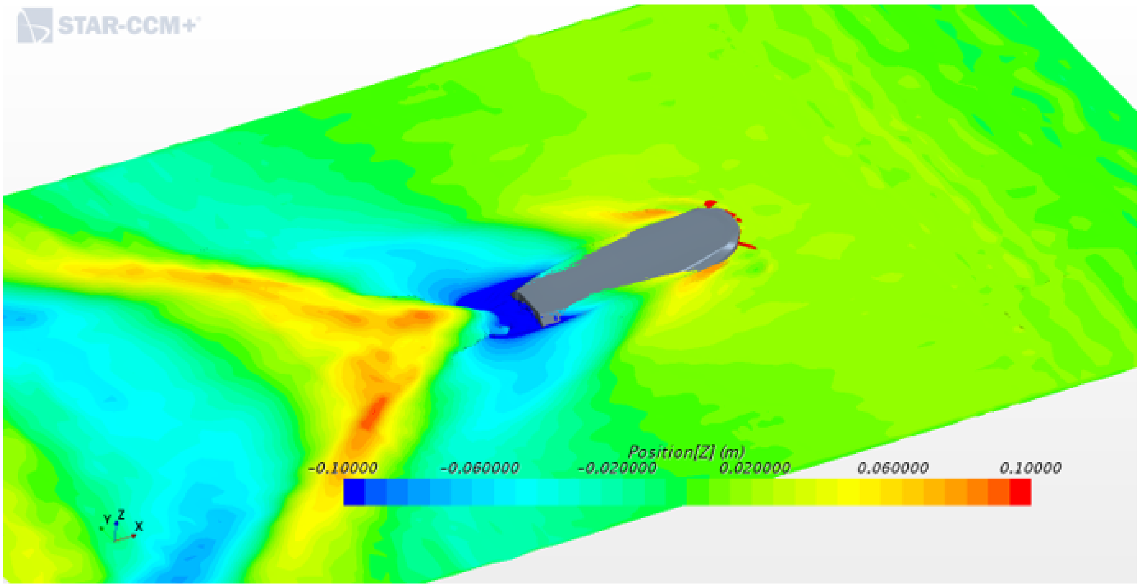

Figure A.1: Free surface for the Wakejet going at 0 RPM at 25 knots with free trim but fixed sinkage.

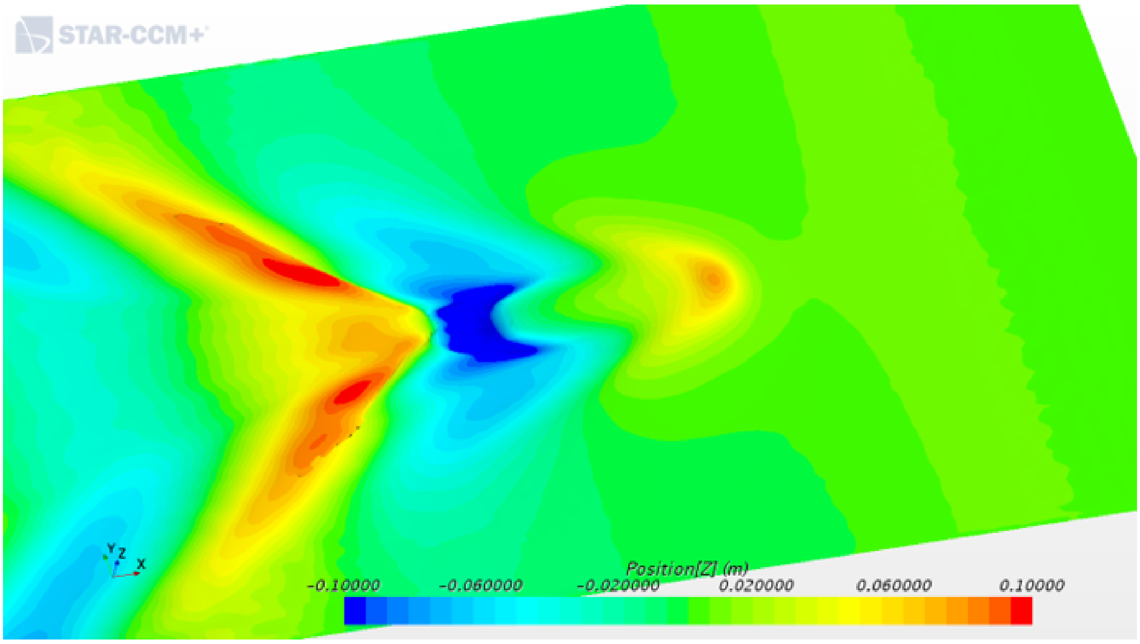

Figure A.2: Free surface for the Wakejet with zero degrees fixed trim and free sinkage going at 0 RPM at 25 knots.